Research Square

Preprints are preliminary reports that have not undergone peer review.
They should not be considered conclusive, used to inform clinical practice,
or referenced by the media as validated information.

AI-assisted synthesis reveals hidden cross-scale degradation in global mangrove ecosystems under human pressure

Mimi Gong

gongmimi@bnu.edu.cn

Advanced Interdisciplinary Institute of Satellite Applications, Beijing Normal University, China

Zhouyi Liu

Beijing Institute of Technology

Yisheng Peng

Sun Yat-sen University

Shen Qu

Beijing Institute of Technology https://orcid.org/0000-0002-8526-3680

Meng Zhang

Advanced Interdisciplinary Institute of Satellite Applications, Beijing Normal University, China

Guoqiang Wang

Beijing Normal University https://orcid.org/0000-0002-4479-7889

Qiao Wang

Beijing Normal University

Article

Keywords:

Posted Date: November 11th, 2026

DOI: https://doi.org/10.21203/rs.3.rs-11135019/v1

License: This work is licensed under a Creative Commons Attribution 4.0 International License.
Read Full License

Additional Declarations: There is **NO** Competing Interest.

AI-assisted synthesis reveals hidden cross-scale degradation in global mangrove ecosystems under human pressure

Abstract

Recent satellite evidence shows that global mangrove extent, after a net loss of ~2,900 km² between the 1980s and 2010, has since rebounded by ~2,000 km², largely through natural seaward expansion and regeneration. Yet this spatial recovery does not necessarily imply the recovery of biodiversity or ecosystem functioning. Satellites record where mangroves grow and species inventories record which organisms persist, but neither captures how plant physiology or metabolism respond to human and climatic pressures beneath the canopy. These responses are measured in thousands of local field and experimental studies, but they remain scattered and unsynthesized at global scale, and pooling them manually has reached practical limits in scalability and traceability. Here, using a human-in-the-loop Retrieval-Augmented Generation (RAG) pipeline, we screened 9,097 articles and built the Quantitative Global Mangrove Biodiversity Risk Database (QGMBRD), compiling 343 independent effect sizes (log response ratios of impacted versus reference conditions) from 6,744 driver-specific studies, spanning landscape to microbial scales under climate change, land-use change, pollution and biological invasion. Despite a nearly fivefold increase in mangrove biodiversity research between 2001 and 2025 (from 1,320 to 6,288 publications). The spatial multilevel meta-analysis further reveals consistent negative responses from macroscopic landscapes to microscopic processes. Crucially, relying solely on traditional taxonomic metrics can yield false-negative conclusions of stability where evidence is scarce and noisy. By contrast, functional metabolic and physiological indicators robustly capture significant degradation and reveal a heavier tail of extreme decline—28.8% of functional observations exceed critical degradation thresholds (|LnRR| > 1), compared with 20.5% for taxonomic metrics. Thus, recent spatial recovery should not be equated with recovery of ecological integrity, global monitoring frameworks must integrate cross-scale functional indicators to diagnose hidden biological impairment. Broadly, our human-centric, AI-augmented framework improves the scalability and traceability of cross-scale ecological evidence synthesis.

1. Introduction

Mangrove ecosystems serve as biological buffers at the land-sea interface, sustaining irreplaceable biodiversity while supplying blue carbon storage and coastal protection[1,2]. After decades of net loss, global mangrove extent has shifted to net gain since around 2010, as accelerating natural seaward expansion and regeneration have increasingly outweighed ongoing losses, with restoration and strengthened protection likely contributing in some regions[3]. This encouraging trend demonstrates substantial spatial resilience, but it does not establish whether biodiversity and ecosystem functions have recovered at the same pace. Mangroves remain exposed to climate extremes and human activities[4-6] , including land-use conversion, chemical pollution, and biological invasions that can reshape internal biogeochemical processes and competitive dynamics[7-9]. Diagnosing these effects therefore demands a macro-scale, integrative framework—the kind of "Continental-Scale Biology" the National Academies of Sciences now envision[9,10].

Recent evidence of mangrove expansion makes this distinction especially important, recovery in spatial extent or canopy cover may not be equivalent to recovery in biodiversity, ecological integrity, or ecosystem functioning[3]. Yet current global evaluation frameworks still rely heavily on remotely sensed spatial extent and localized taxonomic inventories[2,11-13]. Mainstream platforms such as the Global Mangrove Watch track large-scale fluctuations in forest area via satellite imagery[14,15]. Macroecological data infrastructures—including PREDICTS, BioTIME, and the Living Planet Database (LPD)—index long-term trends in species richness or vertebrate population persistence, and bypass basal functional processes altogether[16-20]. These approaches track gross deforestation or broad species loss well, but they capture only presence or absence—not the fine-scale shifts that define ecological health[13]. Mature trees and large fauna can survive chronic stress and preserve a superficial illusion of richness; beneath an intact canopy, an ecosystem's basal metabolic functions and carbon storage capacity may be deteriorate[21]. Broad taxonomic trends

obscure these internal vulnerabilities, and current frameworks risk 'false-negative' conclusions.

Ecological degradation unfolds as a complex, cross-scale process; macroscopic area or simple species persistence alone overlooks the deterioration of underlying ecosystems[22,23]. When mangroves face stressors like localized pollution or extreme climate events, microscopic plant physiology, root metabolism, and soil microbial communities respond rapidly[23,24]. This hidden metabolic and physiological impairment may extend through the coastal food web. Here lies the paradox: forest area and species presence can persist long after the underlying ecosystem crosses its degradation thresholds[23]. This lag, known as "extinction debt," occurs when species persist after habitat quality declines, so taxonomic indicators trail environmental pressure[25]. In high-diversity systems, rare species that support vital ecological functions disappear long before overall species richness shows any decline [26,27]. Two recent case studies show just how far function can drift from structure before either metric raises an alarm. Along North Carolina's coast, declining leaf area preceded a decade-long tree-mortality spike, flagging a coastal forest's shift from carbon sink to carbon source years before the canopy itself visibly failed[28]. On Caribbean reefs, mass coral bleaching left fish-assemblage richness unchanged, yet functional redundancy collapsed as communities converge toward small-bodied, algal-farming generalists—a reorganization that standard richness metrics never caught[29]. Such false-negative assessments—products of overreliance on spatial and taxonomic metrics—undermine our ability to predict and prevent mangroves' silent collapse.

To validate and expose this unseen cross-scale failure, researchers must pool vast amounts of empirical evidence spanning microscopic physiology to macroscopic communities. Existing ecological infrastructures cannot extract high-resolution data from fragmented literature across scales. As environmental science publications grow exponentially, manual literature screening—the traditional method of database construction—has hit its limits. Even the most diligent experts mapping climate-mitigation evidence can process only a fraction of the relevant literature[30]. This labor-intensive process is difficult to scale and may introduce systematic bias from constrained sample sizes[31,32].

Ecology therefore needs scalable and traceable data-mining methods capable of extracting quantitative, cross-scale evidence from non-standardized literature.

To close this gap, we built a human-in-the-loop Retrieval-Augmented Generation (RAG) pipeline to overcome key bottlenecks in traditional evidence synthesis. We processed 6,744 peer-reviewed articles published between 2001 and 2025 and assembled the Quantitative Global Mangrove Biodiversity Risk Database (QGMBRD), which characterizes the mangrove biodiversity literature and compiles independent, cross-scale effect-size samples for assessing responses to human and natural pressures. With QGMBRD, we ask two questions: (1) what patterns of degradation emerge across ecological scales under compounding pressures? and (2) how effectively do current indicators detect this degradation? We show that recent gains in mangrove extent can coexist with biological impairment and that monitoring frameworks should complement spatial and taxonomic inventories with cross-scale functional indicators in conservation and restoration assessments.

2. Results

The widening gap between macro-scale monitoring and local biodiversity measurement.

Mangrove biodiversity research nearly quintupled over the study period, rising from 1,320 publications in 2001–2010 to 6,288 in 2016–2025 (Fig. 1a). Yet the balance of attention across drivers barely moved. Land-use change and climate change together accounted for roughly seven in ten publications across the full 2001–2025 period (35.8% and 34.7% of the four primary driver categories combined, respectively); the two decadal snapshots in Fig. 1a align closely with this figure, at 36% / 34% for 2001–2015 and 36% / 35% for 2016–2025. Each driver grew in near lockstep with the field as a whole: land-use studies rose from 330 to 2,201, climate studies from 329 to 2,127. Pollution research grew at a comparable pace (206 to 1,332), while biological invasion held a narrow and largely stable share of attention throughout the period — near 6.9% of the four driver categories — even as its absolute output rose sixfold, from 61 to 418 studies.

Within land-use research, urbanization has been the dominant pressure throughout the study period, and its lead has widened slightly over time. It accounted for 16.1% of the four primary drivers' output in 2001–2015 (344 of 2,137 records) and rose to 16.5% in 2016–2025 (1,002 of 6,078 records) — in the most recent decade, a volume roughly matching the combined output on agriculture (8.2%, n = 497), extraction and salt-pan development (6.1%, n = 373), and aquaculture (5.4%, n = 329)

A keyword co-occurrence analysis of the same corpus (9,097 records; 98 keywords, 3,824 links, five thematic clusters) traces how the field's vocabulary has moved. Networks built from the earliest years cluster around *community structure* and *seagrass beds* — language describing what a site looks like. By 2017–2018 the vocabulary had shifted toward *management*, *deforestation*, *degradation* and *aquaculture*: the practical work of tracking and mitigating local pressures. By 2019–2020, ahead of the publication surge that followed, *climate change*, *blue carbon*, *ecosystem services* and *sea-level rise* had become the dominant terms — global-change framing had displaced site-level description as the field's organizing language.

That shift has left a gap. Two of the network's most prominent nodes, *blue carbon* and *taxonomy*, never once co-occur across the entire corpus — not a weak link, but no link at all among 3,824 recorded pairings. A related pattern holds for environmental stressors: *aquaculture* sits at the center of a tightly connected cluster of local land-use terms, but its single connection to *pollution* falls below the network's median co-occurrence strength. Mangrove research, in other words, appears to be building two increasingly separate vocabularies — one for counting local biodiversity, another for framing macro-scale monitoring — with surprisingly little traffic between them.

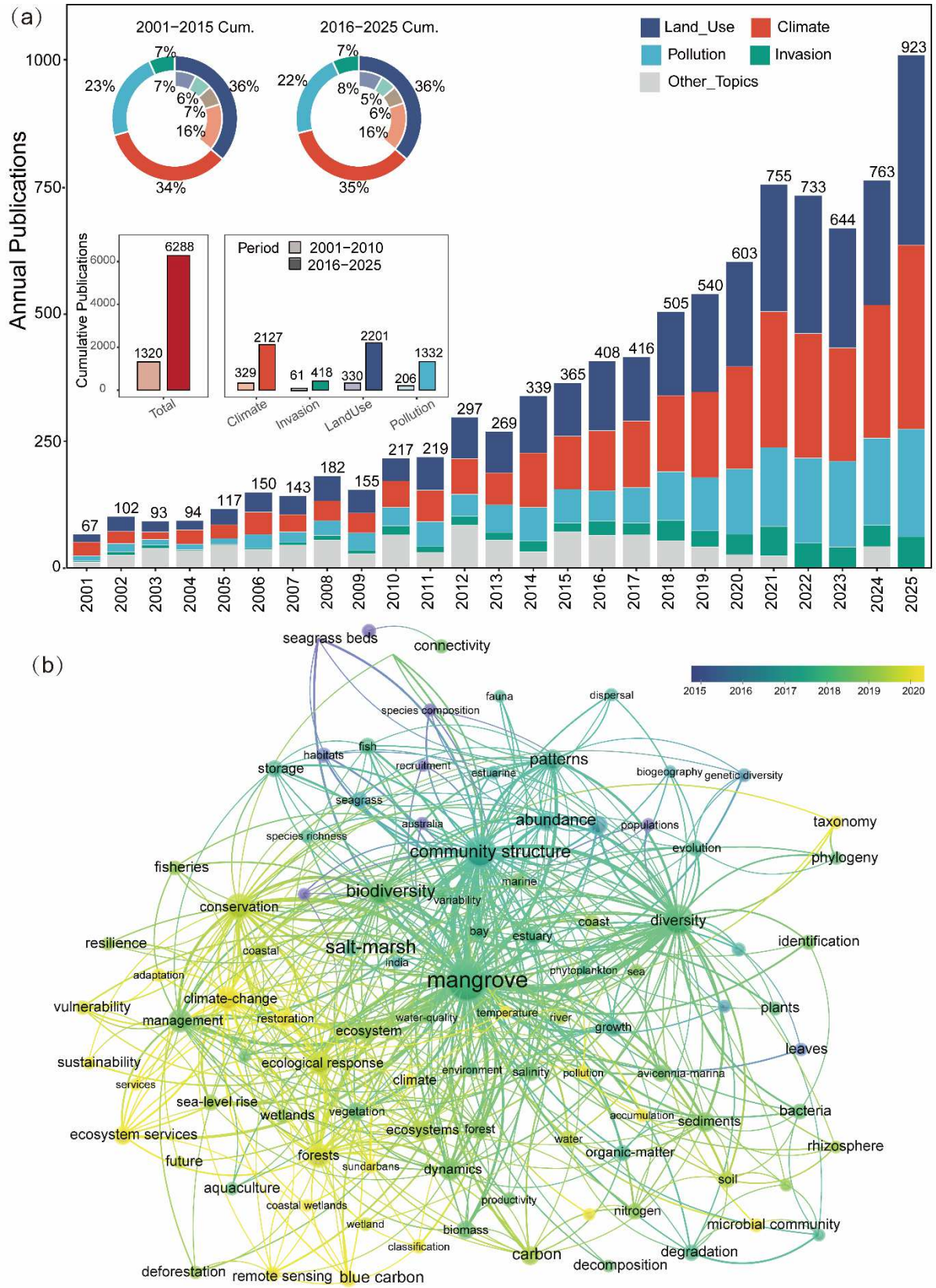


Figure 1 | Research on land-use and climate pressures has scaled in step with mangrove biodiversity research's overall growth, while the field's core vocabulary

has quietly split into two — one describing local ecology, the other framing large scale monitoring. a, While mangrove biodiversity publications grew nearly fivefold between 2001 and 2025 (from 1,320 studies in 2001–2010 to 6,288 in 2016–2025), that growth has not reshuffled the field's priorities: land-use change and climate change have consistently accounted for roughly seven in ten publications across the full study period (35.8% and 34.7% of the four primary driver categories combined). The two decadal snapshots shown here (donut charts, upper left) track closely with that full-period figure, at 36%/34% for 2001–2015 and 36%/35% for 2016–2025. Within land-use research, urbanization has been the largest single contributor in both periods (16.1% and 16.5% of the four-driver total, respectively), and its lead over agriculture, extraction, and aquaculture combined has widened slightly across the two decades. *Note that the outer ring of each donut, and the percentages cited above, are calculated over the sum of the four primary driver categories (land-use, climate, pollution, and invasion); the "Other Topics" segment shown in the stacked bar chart — publications that could not be assigned to one of these four categories — is excluded from all percentage calculations in this figure.* **b,** A keyword co-occurrence network built from the same corpus (9,097 records; title, abstract, and keyword fields only, not full text) shows how the field's core vocabulary has shifted over time. Node size reflects how often a term appears in the literature; connecting lines show which terms tend to appear together in the same studies. Of the terms in this corpus, we retained the 100 with the highest occurrence for network construction, after merging lexical variants via a synonym thesaurus; 98 terms remained after removing non-substantive generic words, connected by 3,824 co-occurrence links. Color traces each term's average publication year, scaled to the 2015–2020 window: publication output rose sharply after 2020, and including the full 2001–2025 range would have pushed nearly every active term toward the same late-period color, obscuring the earlier transition this panel is meant to show. Within that window, terms describing local biological structure (*community structure*, *seagrass beds*) dominate the earliest years; by 2017–2018, practical management terms (*deforestation*, *degradation*, *aquaculture*) take over; by 2019–2020, global-change terms (*climate change*, *blue carbon*, *ecosystem services*, *sea-level rise*) become most prominent. Two of the network's busiest terms, *blue carbon* and *taxonomy*, never once co-occur across the full corpus. *Note that node placement*

and clustering reflect co-occurrence frequency in the literature, not geographic or taxonomic relationships; terms occurring fewer times than the top-100 threshold are not shown and are not implied to be absent from the field.

Global spatial distribution of threat drivers

Across the 34 spatial nodes synthesized here, we catalogued 343 driver-attributed records spanning four dominant stressor categories. Climate was the single most frequently recorded driver globally (156 records, 45.5%), followed closely by land-use change (88, 25.7%) and pollution (86, 25.1%), whereas biological invasion remained rare (13, 3.8%; Fig. 2a). This asymmetry was far from uniform across ocean basins. Nodes in the Americas and wider Atlantic (n = 13) were overwhelmingly climate-dominated—climate accounted for 66% of their records, against only 12% for land-use change and 18% for pollution—while the 21 nodes of the Indo-West Pacific (IWP) displayed a markedly more even stressor composition (climate 34%, land-use 33%, pollution 29%, invasion 4%). Anthropogenic and climatic pressures thus appear to act in far closer concert across the IWP than across the Western Hemisphere.

Four nodes emerged as global hotspots by record count: the Northern South China Sea Shelf (62 records, land-use-dominant), the Ganges–Brahmaputra Delta Shelf (54, climate-dominant), the Southwest Florida Shelf (40, climate-dominant) and the South Puerto Rico Shelf (18, climate-dominant). The Northern South China Sea Shelf was the only one of the four in which land-use change, rather than climate, was the leading driver—consistent with its position within one of the most rapidly urbanizing coastal zones of the IWP. At the network level, climate was the leading driver at half of all nodes (17 of 34), pollution at eight (23.5%), land-use at seven (20.6%) and invasion at only two (the Hawaiian Islands and the Ryukyu Islands, the latter tied with pollution). Invasion-attributed records were confined to just four of the 34 nodes, suggesting that biological invasion is either a genuinely minor pressure on mangrove systems relative to climate and land-use change, or a systematically under-recorded one (see *Gaps and opportunities*, below). Observation density was likewise asymmetric between hemispheres: although 14 of 34 nodes (41%) lay in the Southern Hemisphere, they accounted for only 69 of 343 records (20%), against 274 (80%) across the 20 Northern Hemisphere nodes.

High-resolution structure of land-use pressure in the Indo-West Pacific

Disaggregating the land-use driver into its four constituent sub-categories at high resolution revealed a pattern invisible in the aggregated global map: mining-related

conversion, rather than aquaculture, was the leading land-use sub-category at most IWP nodes for which land-use pressure was recorded (Fig. 2b). Mining accounted for all land-use records at four nodes (the Red Sea, the Gulf of Kutch, the Myanmar–Andaman coast and the Java Sea) and for the majority at two more (the Ganges–Brahmaputra Delta, 49%; the Tanzania coast, 67%). Aquaculture led at only two nodes—exclusively at Palawan and as a co-dominant pressure alongside urbanization at the Northern South China Sea Shelf (34%). Urbanization was concentrated almost entirely at two sites, leading at the Strait of Malacca (86%) and forming the single largest sub-category at the Northern South China Sea Shelf (42%), consistent with the latter's location within an intensely urbanizing estuarine corridor. Agriculture appeared only as a secondary sub-category, never dominant (maximum 40%, at the Ganges–Brahmaputra Delta). Full per-node sub-category counts appear in Supplementary Table X.

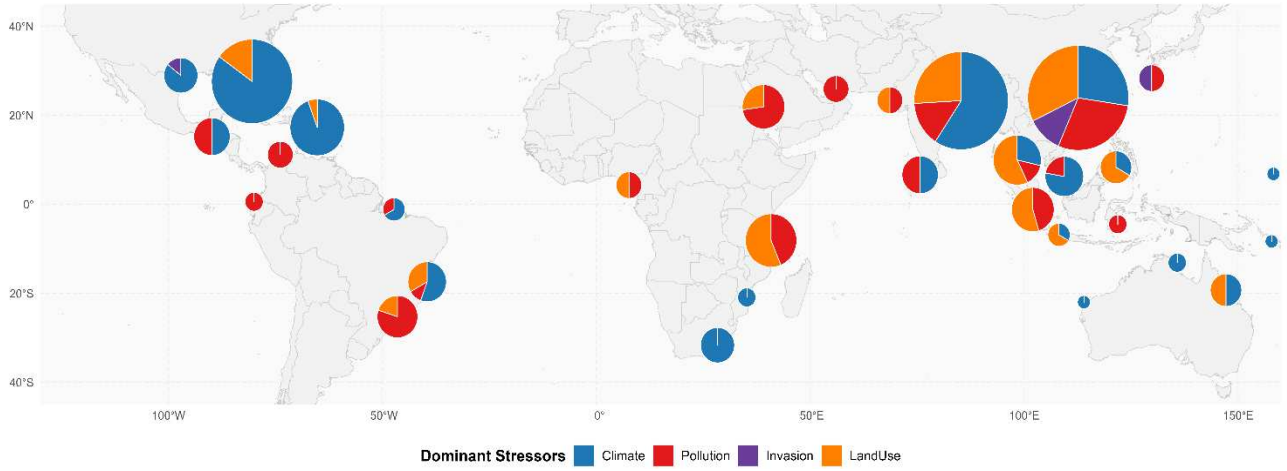
Taxonomic focus and receptor vulnerability

Receptor-resolved data were available for the four highest-intensity hotspot nodes (174 combined records; Fig. 2c). Flora was the most frequently recorded receptor overall (88 records, 50.6%), followed by invertebrates (39, 22.4%), microbiome (29, 16.7%) and vertebrates (18, 10.3%). This aggregate pattern, however, concealed a strong and consistent structuring of taxonomic vulnerability by driver.

Climate-attributed records were overwhelmingly flora-associated at every hotspot, with flora comprising 62–88% of climate records at the Southwest Florida, South Puerto Rico, Ganges–Brahmaputra Delta and Northern South China Sea shelves. Land-use- and pollution-attributed records showed the opposite skew, leaning instead toward microbiome, vertebrate and invertebrate taxa. At the Northern South China Sea Shelf, microbiome accounted for 39% of pollution records and 25% of land-use records—against just 17% and 10% for flora under the same drivers—so that microbiome records marginally exceeded flora there overall (20 vs 19 of 62 records), making it the only hotspot at which a non-flora taxon was the single most-recorded receptor. Vertebrates, by contrast, were entirely unrecorded at the South Puerto Rico Shelf and never exceeded 16% of records at any node, making them the most consistently under-represented receptor across all four hotspots—a gap we return to below. Per-node, per-driver receptor counts are tabulated in Supplementary

Information.

(a)



(b)

(c)

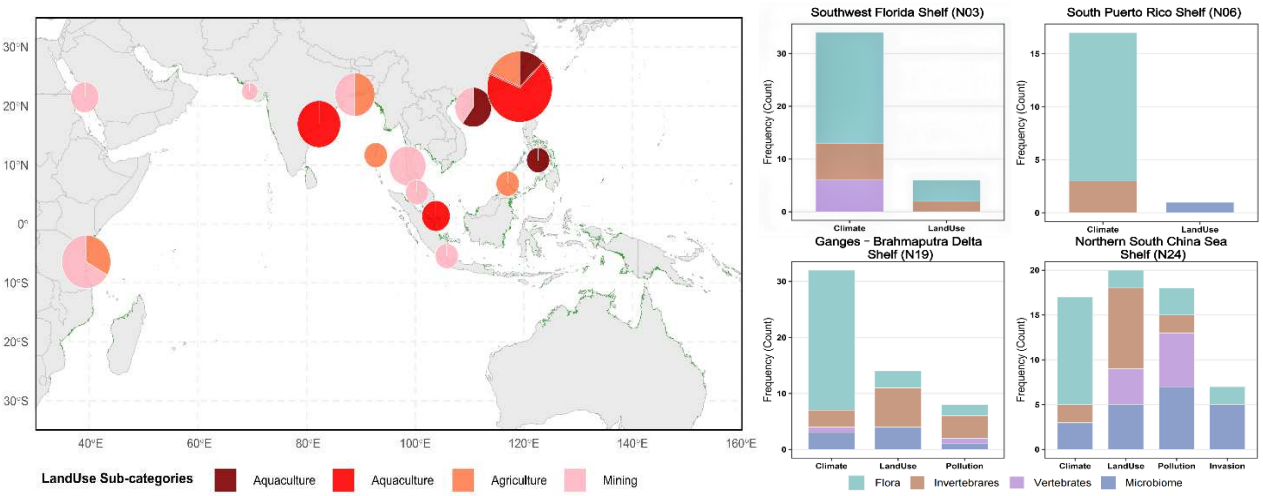


Figure. 2 | Global spatial distribution, sub-categorical land-use pressure, and taxonomic focus of mangrove threat-driver records. a, Global distribution of 34 spatial nodes synthesizing 343 driver-attributed records; pie area scales with total record count per node, and slices give the relative proportion of the four dominant stressor categories (climate, pollution, invasion, land-use). b, High-resolution inset of the Indo-West Pacific (IWP), disaggregating land-use into four sub-categories (aquaculture, agriculture, mining, urbanization); mining—rather than aquaculture—is the leading land-use sub-category at most sampled IWP nodes, most prominently along the Ganges–Brahmaputra Delta, Tanzania and Andaman coasts. c, Frequency of driver-attributed records stacked by receptor taxon (flora, invertebrates, vertebrates, microbiome) at the four hotspot nodes

(Southwest Florida Shelf, South Puerto Rico Shelf, Ganges–Brahmaputra Delta Shelf, Northern South China Sea Shelf); climate-linked records are disproportionately flora-associated at all four, whereas land-use- and pollution-linked records more evenly implicate invertebrate, vertebrate and microbiome taxa. Node identifiers. Place names used in the text correspond to the following node identifiers in Supplementary Table X, which lists coordinates and full driver and receptor counts for all 34 nodes: Northern South China Sea Shelf (N24); Ganges–Brahmaputra Delta Shelf (N19); Southwest Florida Shelf (N03); South Puerto Rico Shelf (N06); northern Gulf of Mexico (N01); Hawaiian Islands (N11); Ryukyu Islands (N28); Red Sea (N14); Gulf of Kutch (N17); Myanmar–Andaman coast (N20); Java Sea (N23); Tanzania coast (N15); Palawan (N26); Strait of Malacca (N21). See Methods for driver and receptor classification criteria.

Spatiotemporal Shifts and Evidence Biases

Our synthesis reveals a research landscape that has expanded rapidly over the past decade yet remains **substantially** uneven in its spatial and thematic coverage. Across every combination of driver and ecological scale, the quantitative evidence accumulated during 2016–2025 overwhelmingly exceeds that of the preceding fifteen years (Fig. 3a). Climate change showed the steepest increase at broad scales, with observations at the landscape and ecosystem scale rising from 4 to 41. Pollution research followed a markedly different spatial signature, concentrating at the micro scale (from 4 to 34 observations), while land-use evidence clustered instead at the community scale (from 9 to 29).

Against this backdrop of growth, biological invasion emerged as a conspicuous evidentiary void. In no single scale-by-period cell does the invasion literature exceed four observations, and the entire 2001–2015 baseline rests on just two records. This scarcity is one of kind rather than degree: relative to climate, pollution, and land use, the existing literature offers no adequate basis for quantitative inference on the impacts of invasion at any ecological scale.

Consistency of Ecological Degradation Across Scales and Metric Types

Evaluated through a continuous effect-size (LnRR) framework rather than a binary

count of significance, the negative responses of mangrove ecosystems proved strikingly consistent across the biological hierarchy. Marginal means for the four ecological scales fell within a narrow band from −0.49 to −0.65; formal pairwise contrasts found no scale differs from another in the magnitude of its response (all Holm-adjusted p = 1.0), and two one-sided equivalence tests confirm this reflects genuine similarity rather than low power — all six full-track contrasts are statistically equivalent within Δ = 0.57 (Δ_min ≤ 0.51), holding under both the primary and the Holm-adjusted threshold (Supplementary Note 5, §5.4, §5.6, §5.8; Tables S10, S12, S16). Crucially, the landscape and ecosystem scale — the tier most often captured by remote sensing — records a decline (LnRR = −0.65) that is statistically equivalent to those at the population, community, and micro scales. Degradation, in other words, is not concentrated at any single level of organization; it unfolds synchronously across the entire system. The same multilevel model shows that climate, land-use, and pollution each drove significant declines in both tracks, whereas biological invasion did not reach significance in either; flora, invertebrates, and vertebrates were all significantly affected, while the microbiome effect was significant only in the full track (Supplementary Note 5, §5.2–5.3; Tables S8–S9). The driver × receptor interaction was comparatively weak, with most cells non-significant or unstable across tracks (Supplementary Note 5, §5.5; Table S11).

This consistency extends to the contrast between taxonomic and functional metrics: a two one-sided equivalence test confirms that the overall Functional − Taxonomic contrast (−0.075, p = 0.565; interaction term $F_{7,323}$ = 0.42, p = 0.89) is statistically equivalent within Δ = 0.57 in both tracks (p_TOST < 0.001), though within-scale equivalence is established only at the community scale and remains undetermined by the current sample at the micro, population, and landscape & ecosystem scales (Supplementary Note 5, §5.7–§5.8; Tables S13, S17). Although functional metrics display a longer and heavier negative tail in their raw distribution — 28.8% of functional observations exceed the severe-degradation threshold of $|\ LnRR\ | > 1$, compared with 20.5% of taxonomic observations, which also explains why the deep-red bubbles appear visually denser in Fig. 3c — their central tendency and cross-group interaction reveal the two metric classes to be equivalent in the magnitude of degradation they record (Supplementary Note 5, §5.7; Table S13.).

One exception is noticed from above uniform picture. Taxonomic metrics at the micro scale (Taxonomic @ Micro) are the only one of the eight metric-type-by-scale combinations for which a significant negative response cannot be resolved (LnRR = −0.43; 95% CI [−1.12, +0.26]; $p = 0.219$). We stress that this reflects not ecological stability at this level, but a severe limitation of the underlying evidence: the estimate rests on only 11 observations, drawn from studies with minimal within-study replication (median $n = 3$) and responses that range from strongly negative to strongly positive. By contrast, functional metrics at the same micro scale (Functional @ Micro), supported by 63 observations, register a highly significant negative response ($p < 0.001$). This disparity exposes the high risk of false-negative assessment inherent in relying on taxonomic metrics alone to gauge mangrove ecological condition at the micro scale.

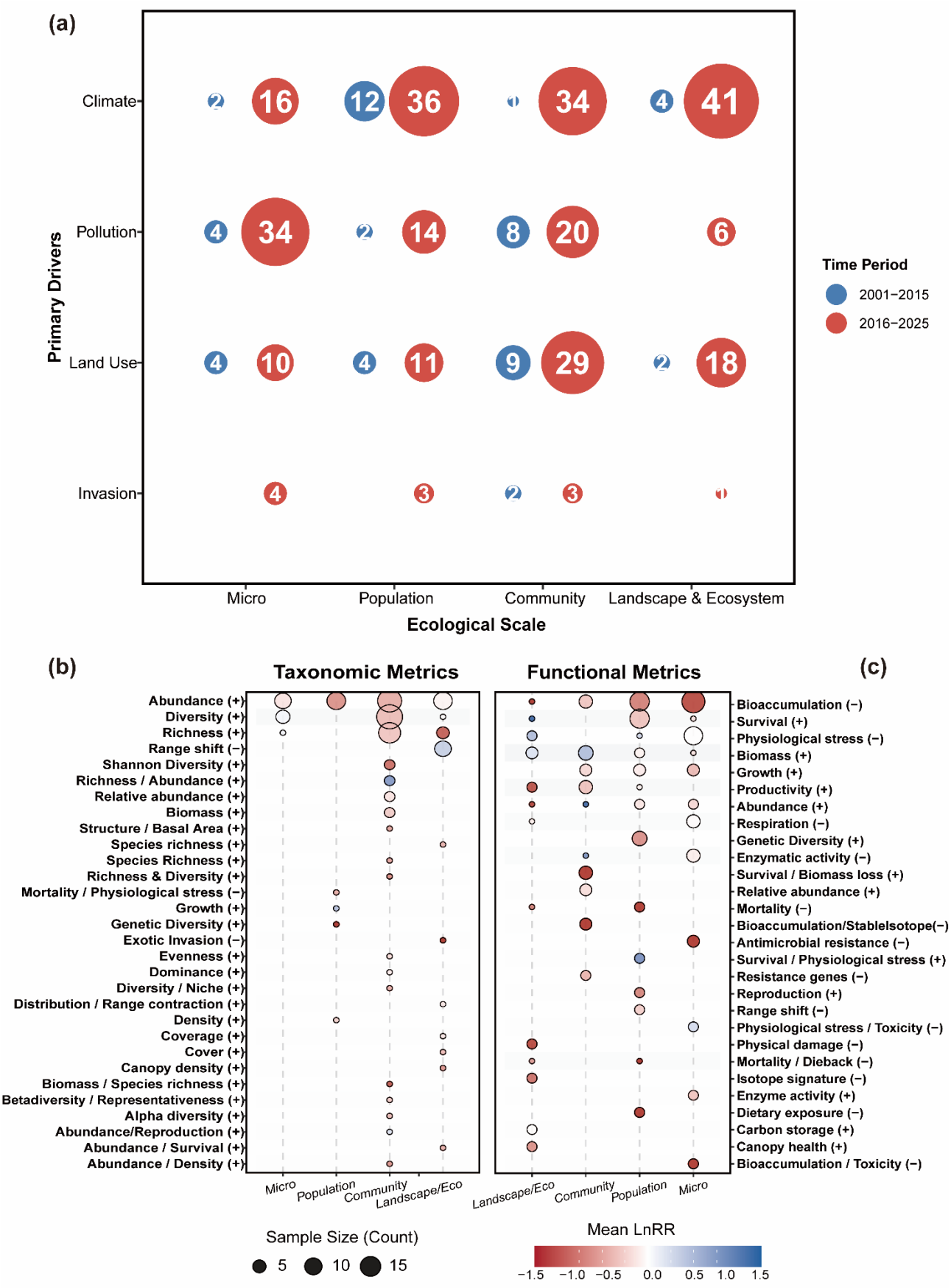

(a)
Climate
Pollution
Land Use
Invasion
Primary Drivers
2 16 12 36 1 34 4 41
4 34 2 14 8 20 6
4 10 4 11 9 29 2 18
4 3 2 3 1
Micro
Population
Community
Landscape & Ecosystem
Ecological Scale
Time Period
2001–2015
2016–2025
(b)
Taxonomic Metrics
Abundance (+)
Diversity (+)
Richness (+)
Range shift (−)
Shannon Diversity (+)
Richness / Abundance (+)
Relative abundance (+)
Biomass (+)
Structure / Basal Area (+)
Species richness (+)
Species Richness (+)
Richness & Diversity (+)
Mortality / Physiological stress (−)
Growth (+)
Genetic Diversity (+)
Exotic Invasion (−)
Evenness (+)
Dominance (+)
Diversity / Niche (+)
Distribution / Range contraction (+)
Density (+)
Coverage (+)
Cover (+)
Canopy density (+)
Biomass / Species richness (+)
Betadiversity / Representativeness (+)
Alpha diversity (+)
Abundance/Reproduction (+)
Abundance / Survival (+)
Abundance / Density (+)
Micro
Population
Community
Landscape/Eco
Functional Metrics
Landscape/Eco
Community
Population
Micro
(c)
Bioaccumulation (−)
Survival (+)
Physiological stress (−)
Biomass (+)
Growth (+)
Productivity (+)
Abundance (+)
Respiration (−)
Genetic Diversity (+)
Enzymatic activity (−)
Survival / Biomass loss (+)
Relative abundance (+)
Mortality (−)
Bioaccumulation/StableIsotope(−)
Antimicrobial resistance (−)
Survival / Physiological stress (+)
Resistance genes (−)
Reproduction (+)
Range shift (−)
Physiological stress / Toxicity (−)
Physical damage (−)
Mortality / Dieback (−)
Isotope signature (−)
Enzyme activity (+)
Dietary exposure (−)
Carbon storage (+)
Canopy health (+)
Bioaccumulation / Toxicity (−)
Sample Size (Count)
5
10
15
Mean LnRR
−1.5 −1.0 −0.5 0.0 0.5 1.0 1.5

Figure 3. Degradation occurs synchronously across all ecological scales, yet the underlying evidence is structurally skewed and weakest where sensitivity is most critical. (a) The spatiotemporal expansion of mangrove biodiversity research is characterized by a persistent evidence imbalance. While publication volume has surged since 2016 (red bubbles), research effort remains siloed: climate change studies dominate the landscape scale, whereas pollution and land-use research are heavily concentrated at micro- and community-level resolutions. Biological invasion remains a critical evidentiary void, with research efforts never exceeding four observations in any single scale–period cell. (b, c) Taxonomic and functional metrics record statistically equivalent magnitudes of ecological decline across the biological hierarchy, providing positive evidence against a gradient-based decline. The visual intensity in the functional panel (c) — marked by deep-red bubbles for bioaccumulation and physiological stress — reflects a heavier distribution of extreme negative responses (28.8% of observations with $|LnRR| > 1$) rather than a stronger mean effect relative to taxonomic metrics ($p = 0.50$). The only combination failing to register a significant decline is Taxonomic @ Micro; this absence of statistical resolution is not evidence of ecological stability, but an artifact of extreme under-sampling ($n = 11$, median within-study $n = 3$) that highlights a systemic blind spot in current taxonomic monitoring protocols.

3. Discussion

Here we synthesize the mechanistic pathways through which anthropogenic and climatic pressures degrade mangrove biodiversity concurrently across biological scales. Consistent with our finding that degradation is statistically indistinguishable in magnitude across ecological scales (Fig. 4), these pathways operate not as a top-down cascade but as simultaneous, scale-specific manifestations of the same stressors — with the crucial distinction that degradation is often masked at the taxonomic level even as it advances functionally.

Physical restructuring of the coastal margin

Anthropogenic infrastructure and extreme physical disturbances disrupt the macroscopic hydrologic connectivity of coastal margins[33-36]. Intact mangrove ecosystems naturally buffer tidal fluctuations via gradual topographic transitions, whereas engineered seawalls truncate this elevation gradient [37,38]. These structures create hard barriers that restrict the inland migration of habitats during sea-level rise [39,40], directly driving a structural coastal squeeze [41,42]. Crucially, barriers of a different physical nature, but with comparable consequences for habitat continuity, also arise at the micro-habitat level through unmanaged anthropogenic effluents [43-49]. Macro-plastic debris accumulates along tidal fringes[50,51], a physical barrier over benthic sediments [52-56]. This continuous layer inflicts persistent mechanical friction damage on mangrove pneumatic roots. Localized empirical assessments highlight the severity of these micro-scale blockages, recording plastic densities of up to 1.38 items/m² under specific environmental pressures on the mangrove ecosystem in Negombo Lagoon[57].

Beyond coastal infrastructure, upstream damming and channel dredging further sever hydrological pathways[58-63]. The resulting substrate siltation restricts resource availability within the detrital food web. In Kakinada Bay, for example, this isolation drove a precipitous decline in detritus feeders from 62.12% to 20.23%[64]. When these spatially restricted systems

face extreme climate pulses like hurricanes, structural damage extends into the substrate[65-71]. Category-4 hurricanes, for instance, induce up to 50% mortality in large-diameter canopy trees. This massive forest dieback directly collapses the underlying peat root mat and causes significant soil elevation loss[72,73]. Furthermore, climate-driven tropicalization initiates gradual physical restructuring even without acute climate events[74-77]. The competitive expansion of woody vegetation systematically displaces grass- and forb-dominated habitats. This ecological regime shift fundamentally alters the vertical architecture of the coastal ecosystem[78-81].

Abundance without integrity

We also recognize that the ecological assessment on macro-scale abundance may mask the status change of biodiversity structure on micro scales. Traditional ecological assessments frequently equate high taxonomic abundance or dense vegetative cover with ecosystem stability[82-87]. However, these absolute density metrics often obscure the underlying degradation of food web architecture and the shift toward smaller organism sizes[88,89]. For example, the establishment of exotic *Spartina alterniflora* in estuaries significantly increased benthic organism density from 669 to 1,398 ind./m²[90]. This numerical surge, however, was driven entirely by the rapid proliferation of small, opportunistic polychaetes. Behind this apparent biological abundance, the ecosystem actually experienced a severe reduction in total benthic biomass and the competitive exclusion of native surface deposit-feeders[90-92].

Aquaculture effluent stress induces a similar structural shift. Although overall taxonomic density remains unchanged, total community biomass declines by 40%, marking a clear transition toward smaller, lower-trophic r-strategists[45]. This decoupling — functional collapse beneath an unchanged taxonomic surface — is the mechanistic signature of the pattern quantified in Fig. 3 b, c, where functional and taxonomic metrics record statistically equivalent mean responses yet functional metrics capture a heavier tail of extreme distress. Similarly, urban runoff introduces substantial nitrogen and phosphorus into estuaries82-86. These nutrient subsidies sustain high-density vegetative canopies, projecting a false image of ecological health[93-97]. In reality, this robust vegetation obscures the concurrent

accumulation of sediment toxicity[98,99].

Beneath these continuous canopies, heavy metal pollutants transfer from sediments to invertebrates and ultimately biomagnify in top-tier migratory shorebirds. This process compromises the apex of the food web through high trophic magnification factors (TMF), even while basal primary production appears completely stable[16,100-104]. Ultimately, this superficial stability leaves the ecosystem highly vulnerable to extreme climate pulses[70,105-108]. Extreme cold incursions, for instance, deplete basal resources and severely shrink the ecological niche breadth of benthic communities[70,109]. As a result, taxonomic richness drops sharply from 24 to 13 species, driving a profound simplification of the coastal food web[110].

Metabolic and genetic failure at the sub-organismal scale

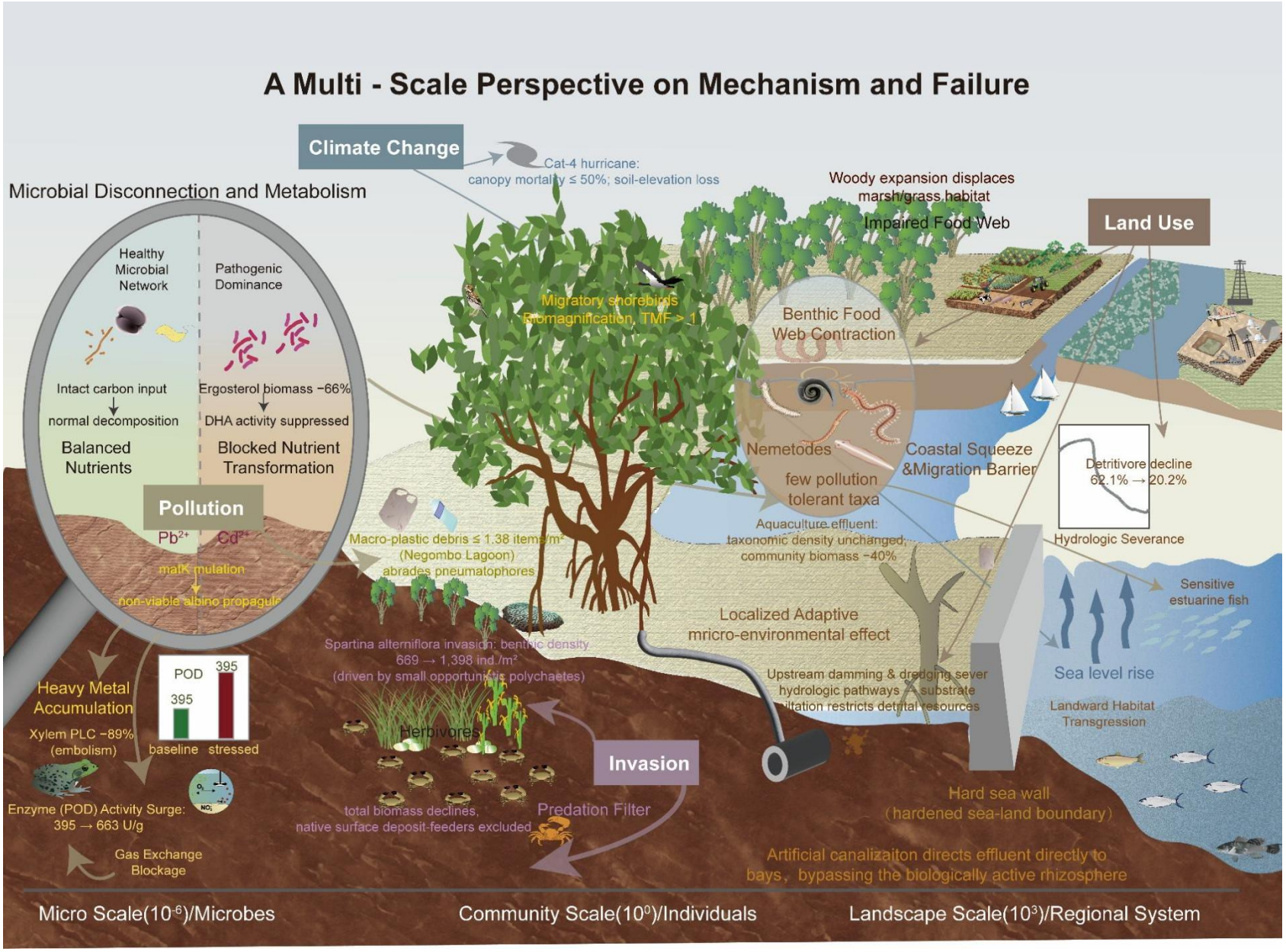
Unmitigated landscape-scale pressures are accompanied by, rather than followed by, losses of micro-scale integrity. This sustained stress decouples intracellular metabolism from ecosystem-level biogeochemical cycling[111,112]. For example, converting native mangroves to agricultural land interrupts essential subsurface carbon inputs. This physical disruption reduces fungal ergosterol biomass by 66% and suppresses heterotrophic dehydrogenase (DHA) activity, driving a systemic decline in overall microbial metabolism[113]. Furthermore, chronic chemical exposure fundamentally alters genetic and physiological baselines. Prolonged exposure to polycyclic aromatic hydrocarbons (PAHs) induces mutations within nuclear and chloroplast genes, such as *matK*. These genetic damages directly trigger the production of completely non-viable albino propagules[114]. Similarly, sublethal cadmium contamination disrupts root-microbe interactions by driving the enrichment of iron-oxidizing bacteria (FeOB). The plant relies on these recruited bacteria to form protective iron plaques, an active defense mechanism that forces a severe reallocation of the plant's energy resources[115].

These metabolic constraints are exacerbated when compounded by severe climate pulses.

Low-temperature incursions breach the thermal thresholds of photosystem II. In sensitive species, temperatures near -4.4 °C trigger severe tissue necrosis and total foliar mortality[116]. Simultaneously, high temperatures and reduced tidal inundation create severe

moisture deficits that lower soil water potential. This precipitates hydraulic failure, causing an 89% loss of xylem conductivity through massive vessel embolism[117]. At the enzymatic level, chemical and radiation stressors compound this physiological collapse. Sub-lethal heavy metal toxicity disrupts membrane integrity and denatures essential enzymes. To mitigate the resulting oxidative damage, plants overproduce reactive oxygen species (ROS), forcing peroxidase (POD) activity to surge from 395 to 663 U/g[118]. Similarly, extreme ultraviolet radiation induces a 6-fold increase in intracellular ROS production. This oxidative stress inflicts 37% DNA double-strand breaks in bacterial cells, severely impairing fundamental microbial functions[119].

Figure 4 summarizes these pathways, illustrating how the same anthropogenic and climatic pressures manifest **concurrently across scales — from macroscopic vegetation shifts to microscopic metabolic failure — rather than propagating unidirectionally between them**. Critically, because these processes unfold in parallel, degradation registered by any single scale or metric class reflects a system-wide condition, not an isolated or leading indicator.


A Multi - Scale Perspective on Mechanism and Failure
Climate Change
Cat-4 hurricane:
canopy mortality ≤ 50%; soil-elevation loss
Microbial Disconnection and Metabolism
Healthy Microbial Network
Pathogenic Dominance
Intact carbon input
normal decomposition
Balanced Nutrients
Ergosterol biomass −66%
DHA activity suppressed
Blocked Nutrient Transformation
Pollution
Pb2+
Cd2+
malK mutation
non-viable albino propagule
Woody expansion displaces marsh/grass habitat
Impaired Food Web
Land Use
Migratory shorebirds
Biomagnification, TMF > 1
Benthic Food Web Contraction
Nemetodes
few pollution tolerant taxa
Coastal Squeeze &Migration Barrier
Detritivore decline
62.1% → 20.2%
Hydrologic Severance
Aquaculture effluent:
taxonomic density unchanged,
community biomass −40%
Macro-plastic debris ≤ 1.38 items/m²
(Negombo Lagoon)
abrades pneumatophores
Localized Adaptive
mricro-environmental effect
Sensitive estuarine fish
Spartina alterniflora invasion: benthic density
669 → 1,398 ind./m²
(driven by small opportunistic polychaetes)
Upstream damming & dredging sever hydrologic pathways ↓ substrate
siltation restricts detrital resources
Sea level rise
Landward Habitat Transgression
Heavy Metal Accumulation
Xylem PLC −89%
(embolism)
POD
395
395
baseline
stressed
Herbivores
Invasion
Enzyme (POD) Activity Surge:
395 → 663 U/g
total biomass declines,
native surface deposit-feeders excluded
Predation Filter
Hard sea wall
(hardened sea-land boundary)
Gas Exchange Blockage
Artificial canalizaiton directs effluent directly to bays, bypassing the biologically active rhizosphere
Micro Scale(10-6)/Microbes
Community Scale(10⁰)/Individuals
Landscape Scale(10³)/Regional System

453

Figure 4 | Systemic propagation of anthropogenic and climatic stressors across mangrove biological hierarchies. This conceptual framework illustrates the pervasive penetration of ecological stress. Anthropogenic pressures do not merely cascade across scales; they act synchronously across all organizational levels. Macro-scale anthropogenic infrastructure (e.g., seawalls, debris) and upstream hydrological disruptions (e.g., damming) interact with localized stressors (e.g., chemical toxicity, extreme climate pulses) to drive systemic degradation. Rather than functional erosion acting as a temporal precursor to structural loss, our synthesis reveals that physiological failure (e.g., metabolic arrest, xylem embolism, genetic damage) and structural decline (e.g., biomass loss, diversity reduction) manifest concurrently. The lack of sensitivity detected in taxonomic micro-scale monitoring (as seen in Figure 3) is more plausibly attributed to limited observational sensitivity than to an absence of ecological stress; therefore, this framework emphasizes that any indicator of degradation—whether at the microbial or landscape scale—must be treated as a signal of systemic vulnerability.

Why taxonomic and functional metrics are not interchangeable

The global degradation of mangrove ecosystems registers at a consistent magnitude across all biological hierarchies rather than at any single level. Our meta-analysis reveals that anthropogenic pressure does not merely affect isolated components; it drives a pervasive decline of comparable magnitude from landscape-level structural loss to microscopic metabolic failure. This consistency across scales suggests that the mangrove ecosystem behaves as a tightly coupled system in which the degradation of functional integrity and the loss of structural complexity are closely associated.

The most profound insight from our synthesis lies in the conceptual decoupling of taxonomic abundance from functional integrity. While equivalence testing establishes that taxonomic and functional indices record the same mean effect size (Supplementary Note 5, §5.8; Table S17), this equivalence should not be interpreted as functional redundancy. Rather, it exposes a critical limitation in current ecological monitoring: reliance on taxonomic counts (e.g., species richness, total abundance) provides only a surface-level census of the ecosystem. Such metrics effectively track the *inventory* of the ecosystem, but they are conceptually blind to the *mechanistic truth* of its health. As our data demonstrates, an ecosystem can maintain superficial taxonomic stability while its core biogeochemical and metabolic engines are already in advanced stages of decay.

The unique diagnostic value of functional metrics is best revealed by their distributional profile, which captures the most extreme physiological shocks to the ecosystem. While taxonomic indices often cluster around moderate response magnitudes, functional metrics exhibit a significantly heavier tail of extreme degradation—with 28.8% of observations falling below a severe impairment threshold of LnRR = −1, compared to only 20.5% for taxonomic metrics. This distributional difference suggests that functional indicators are not merely "more sensitive"; they are fundamentally distinct instruments. They operate at the level of direct evidence—capturing bioaccumulation, enzymatic suppression, and metabolic arrest—which taxonomic inventories simply cannot resolve. When the ecosystem is pushed to the brink, functional metrics record physiological impairment directly, whereas taxonomic counts often fail to differentiate between thriving communities and those sustained by

opportunistic, stress-tolerant generalists.

The micro-scale evidentiary blind spot

This failure of taxonomic metrics is most starkly evident at the micro-scale, where the current evidence base for structural change is essentially compromised. The non-significant response observed in Taxonomic @ Micro observations is consistent with this conceptual blind spot, although the present evidence cannot yet distinguish genuine micro-scale stability from a response that current sampling designs are unable to detect. Interpreted without this caveat, reliance on basal taxonomic counts at this scale invites systemic "false-negative" assessments, as the directional variance of taxonomic composition is high while the corresponding functional deterioration is highly significant ($p < 0.001$). Taxonomic metrics, in this context, act as a noisy background signal that masks the precise, metabolic decline of the ecosystem.

Ultimately, these findings necessitate a paradigm shift in how we operationalize mangrove conservation. We must move beyond the "surface-level audit" approach of tracking species counts or canopy cover. The erosion of functional processes—such as nutrient cycling, root metabolism, and trophic energy transfer—is the definitive indicator of ecosystem health. Future management frameworks must prioritize the monitoring of these basal functional dynamics. By integrating functional assays (e.g., physiological, genetic, and enzymatic indices) alongside traditional surveys, we can bridge the gap between apparent biological abundance and the underlying functional reality, ensuring that conservation efforts are directed at the metabolic stability—rather than just the superficial inventory—of global mangrove ecosystems.

Implications for monitoring and conservation

Our synthesis exposes where the global evidence base is strong, where it is thin, and where it is missing entirely. Building on these patterns, we pose the following questions to advance the monitoring, theory and management of mangrove ecosystems in the Anthropocene:

1. **How can monitoring frameworks integrate functional metrics — metabolic**

stability, trophic structure, energy flow — alongside the structural and taxonomic measures that currently dominate? Because functional and taxonomic signals are statistically equivalent in magnitude yet conceptually distinct, neither substitutes for the other.

2. **What sampling designs would close the micro-scale evidentiary blind spot?** Raising within-study replication for sub-organismal and microbial metrics, rather than accumulating further single-observation studies, is the most direct route to resolving whether apparent micro-scale stability is real or merely unmeasured.
3. **How should research effort be redistributed toward biological invasion before its impacts become unquantifiable?** With no scale-by-period cell exceeding four observations, invasion remains the single largest thematic void in the mangrove evidence base — a gap that widens as warming accelerates the spread of novel invaders.
4. **Can conservation act on continuous evidence of degradation rather than on thresholds of statistical significance?** Because decline in our synthesis is a matter of consistent magnitude rather than scattered significant results, management triggered by the weight of evidence — effect size and its precision — would respond earlier than management that waits for individually significant losses.
5. **How can the mismatch between research attention and extractable evidence be corrected at the point of study design?** Standardized reporting of means, variances and sample sizes would convert today's uneven coverage into a usable global evidence base, particularly for the data-poor micro-habitats where structural assessment currently fails.

4. METHODS

4.1 Literature search strategy and shared definitions (Track A and Track B)

Our study rests on two independent Web of Science searches. Track A is an overview search: it characterizes the mangrove-biodiversity literature as a whole, tracing its growth, thematic structure, and temporal shifts (Figure 1), and it establishes the two definitions shared by both tracks: mangrove (the ecosystem block, built from the 19 true mangrove genera) and biodiversity (a fixed 12-term response vocabulary spanning diversity indices, demographic measures, and community structure). Track B applies this same mangrove-and-biodiversity core against four driver-specific blocks (climate change and extreme weather, pollution, biological invasion, and land-use change) to extract the quantitative, driver-resolved evidence used in the meta-analysis (§4.2). The two tracks share an identical mangrove and biodiversity vocabulary and differ only in whether a driver term is added, so any difference between them reflects the literature itself rather than inconsistent search scope.

Queries were executed on the Topic/Keyword field on 5 April 2026, which matches an article's title, abstract, and author keywords. Query construction followed Web of Science's Boolean and truncation rules: synonyms within one dimension were joined by **OR** into a term block (union), blocks from different dimensions were combined by **AND** (intersection), and word stems were truncated with an asterisk (*) to capture all inflectional and derivational variants (e.g. *diversit** matches *diversity* and *diversities*). Searching the keyword field rather than full text ensures that retrieved articles genuinely *treat* mangroves and their biodiversity as a subject rather than merely mentioning them in passing; the combination of within-block union, between-block intersection, and stem truncation balances precision (the intersection constrains topicality) against recall (union and truncation maximize retrieval) over the "mangrove ∩ biodiversity-response" semantic intersection.

Track A combined the ecosystem block with the biodiversity block by AND to maximize

recall of the trend literature, returning **9,097 articles**, used solely for the Figure 1 **Ecosystem dimension (Block A)** is *mangrove** joined by OR to the 19 true-mangrove genera, each truncated (e.g. *Acanthus**): Acanthus, Acrostichum, Aegialitis, Aegiceras, Avicennia, Bruguiera, Camptostemon, Ceriops, Excoecaria, Kandelia, Laguncularia, Lumnitzera, Nypa, Osbornia, Pelliciera, Rhizophora, Scyphiphora, Sonneratia, Xylocarpus.

Biodiversity dimension (Block B) is a fixed 12-term block held identical across all four drivers, so that search scope is strictly comparable across stressors: *biodivers**, alpha, gamma, beta, *diversit**, *communit**, Species richness, Abundance, Mortality, *Survival rate**, *Shannon**, Basal area. It targets within-stand biodiversity and demographic responses and deliberately excludes area, extent, and cover: because the study tests whether area-based macro-proxies mask fine-scale ecological change, admitting those proxies into the response block would conflate the response variable with the macro-scale metric under scrutiny.

The block was designed for both scientific representativeness and dimensional completeness, systematically covering three core levels of the mangrove biodiversity response. First, a **diversity-index level** — α, β, and γ diversity across spatial scales, together with the Shannon index and species richness — characterizes community species composition. Second, a **demographic level** — abundance, mortality, and survival — captures population dynamics. Third, a **community-and-structural level** — community composition and basal area — reflects the stand-level response. Together these three levels ensure the search captures both taxonomic, species-inventory signals and functional, population- and structure-level signals, providing a sufficient and balanced evidentiary basis for the downstream distinction between taxonomic and functional responses. Stem truncation (e.g. *diversit**, *communit**) further maximizes recall by admitting cognate word-form variants (Full genus list and the two search-track comparison are given in Supplementary Note 1, Tables S1–S2.).

Keyword co-occurrence network construction and temporal overlay visualization

Using the bibliographic records of all 9,097 Track A articles as input, we built a keyword co-occurrence network in VOSviewer 1.6.20[120]. This analysis draws on the Track A corpus only, involves no driver-restricted query, and aims to characterize the overall thematic structure and temporal evolution of mangrove-biodiversity research rather than its driver-

resolved composition. VOSviewer's mapping logic comprises three sequential stages — co-occurrence counting and similarity normalization, similarity-based layout and clustering, and attribute overlay coloring on the resulting topology. All three share one similarity matrix, a structural fact that is the precondition for the later temporal-scale recalibration to leave the network topology untouched.

Co-occurrence counting and association-strength normalization. Let the corpus contain n keywords retained for analysis, and let c_{ij} be the number of documents in which keywords i and j co-occur, under full counting (each document contributes one co-occurrence to every keyword pair it contains). Write $v_i = \sum_j c_{ij}$ for the total link strength of keyword i, and $k = 1/2 \sum_i v_i$ for the total number of co-occurrence events. Raw co-occurrence frequencies are strongly confounded by a keyword's own frequency — high-frequency words co-occur with everything — which can mask genuine thematic affinity. VOSviewer therefore normalizes by the **association strength**[120]:

$$s_{ij} = \frac{2k\, c_{ij}}{v_i\, v_j}$$

The numerator is the observed number of co-occurrences and the denominator is proportional to the number expected under the null hypothesis that the two keywords are independent, so s_{ij} is an observed/expected ratio: $s_{ij} > 1$ indicates that the two words co-occur substantially more than random expectation. This normalization prevents low-frequency but thematically bound pairs from being drowned out by high-frequency generic terms, and is what allows the network to reflect conceptual structure rather than mere word frequency.

Layout. Node coordinates are not arbitrary but the solution of a constrained weighted-stress minimization. VOSviewer solves for coordinates $x_i \in \mathbb{R}^2$ minimizing:

$$L(x_1, \ldots, x_n) = \sum_{i<j} s_{ij} \parallel x_i - x_j \parallel^2$$

subject to the constraint that the mean Euclidean distance over all pairs is fixed to one,

$$\frac{2}{n(n-1)} \sum_{i<j} \parallel x_i - x_j \parallel = 1;$$

the constraint excludes the trivial solution in which all points collapse to a single location

and makes the solution unique up to similarity transforms, solved by a majorization algorithm. Its direct meaning is that **the Euclidean distance between two keywords is approximately inversely proportional to their thematic relatedness** — the closer, the stronger the association. This contrasts with force-directed layouts (e.g. Fruchterman–Reingold), whose inter-node distances carry no explicit metric interpretation and thus cannot support inferences about thematic proximity.

Clustering. Clustering shares the same similarity matrix as the layout, solved in a unified framework. Writing c_i for the cluster label of keyword i, we maximize:

$$L(c_1, \ldots, c_n) = \sum_{i<j} \delta\left(c_i, c_j\right)\left(s_{ij} - \alpha\right)$$

where $\delta(\cdot,\cdot)$ is the Kronecker function (1 within a cluster, 0 between) and α is a resolution parameter controlling cluster granularity — larger α yields more and smaller clusters. We used the default resolution $\alpha = 1.00$ and a minimum cluster size of 1, solved by the smart local moving algorithm[121]. Because clustering and layout objectives are built on the same s_{ij}, spatial proximity and cluster colouring are highly self-consistent in the map, which is what makes “nodes far apart in space with weak links” a formal basis for inferring thematic disconnection.

Threshold and thesaurus cleaning. We set a minimum keyword occurrence of 80 and, among terms meeting that threshold, retained the top 100 by occurrence; after merging word-form variants with a thesaurus and removing constructive query terms and non-informative generic words, the final map contains **98 keyword nodes and 3,824 co-occurrence links**, resolving into **5 clusters**. Node area is proportional to keyword occurrence and link width to co-occurrence strength. The network’s link density is 0.805 (3,824 of 4,753 possible node pairs co-occur), indicating that mangrove-biodiversity research is highly interconnected at the lexical level; accordingly, all later arguments about thematic disconnection rest on **weighted link strength** rather than the presence or absence of links.

Temporal overlay visualization and the mathematics of its colouring. To resolve the temporal evolution of thematic structure, we rendered an overlay visualization colouring each keyword by its **mean publication year**. Let D_i be the set of documents containing

keyword i and y_d the publication year of document d; then

$$\bar{y}_i = \frac{1}{|D_i|} \sum_{d \in D_i} y_d.$$

VOSviewer maps this scalar score to a continuous colour scale after linear normalization. With the scale defined over $[a, b]$, the normalized colour position of keyword i is

$$z_i = \mathrm{clip}\left(\frac{\bar{y}_i - a}{b - a},\ 0,\ 1\right),$$

followed by piecewise-linear RGB interpolation over palette control points $\{(z_k, C_k)\}$:

$$C(z) = C_k + \frac{z - z_k}{z_{k+1} - z_k}\,(C_{k+1} - C_k), \qquad z \in [z_k, z_{k+1}].$$

The software default takes $a = \min_i \bar{y}_i$ and $b = \max_i \bar{y}_i$, i.e. it auto-stretches the scale to the extreme observed scores. This default loses substantial resolution for the present corpus, for a reason that follows directly from the construction of $\bar{y}_i$. Writing $n_i(y)$ for the occurrences of keyword i in year y,

$$\bar{y}_i = \frac{\sum_y y\ n_i(y)}{\sum_y n_i\,(y)}, \qquad n_i(y) = N(y)\,\pi_i(y),$$

where $N(y)$ is the corpus's total annual output and $\pi_i(y)$ the occurrence rate of keyword i that year. Because $N(y)$ rises steeply over 2021–2025, **the weighted mass of every keyword is systematically pushed toward the recent end of the time axis regardless of each keyword's own temporal shape** $\pi_i(y)$, shifting $\{\bar{y}_i\}$ to the right and compressing between-keyword dispersion. The empirical distribution confirms this: the 98 keywords' $\bar{y}_i$ span 2014.07–2021.65 (range 7.58 years) yet have a standard deviation of only 1.51 years and an interquartile range (IQR) of only 1.81 years, with a distribution skew of −0.60 — a left-skewed shape in which a few early keywords form a sparse left tail while the bulk piles up near the recent end. Under the default extreme auto-stretch, 66.3% of nodes have $z_i \geq 0.5$, and the IQR spans only 0.238 of the colour scale — that is, the temporal differences among half the keywords are compressed into less than a quarter of the colour budget, appearing as large blocks of near-identical colour with an illegible temporal gradient.

We therefore **replaced the extreme auto-stretch with a fixed interval**, setting the colour-scale definition to $[a, b] = [2015{,}2020]$. This is equivalent to a linear contrast stretch of the $\bar{y}$ distribution with double-sided winsorization of values outside the interval: 80 of the

98 nodes (81.6%) fall within the interval and receive full colour resolution, while 5 and 13 nodes are clipped to the low and high scale ends respectively; the IQR's share of the colour scale rises from 0.238 to 0.361 (1.52× the default), unfolding the temporal differences within the dense central band. After recalibration, the temporal centroids of the clusters separate cleanly along the scale into a continuous chain of thematic turnover: community and habitat themes (Cluster 2, mean $\bar{y} = 2017.06$) and species and evolution themes (Cluster 3, mean $\bar{y} = 2017.44$) at the early end, biogeochemical-process themes (Cluster 4, mean $\bar{y} = 2018.88$) in the middle, and macro-scale climate-change and ecosystem-service themes (Cluster 1, mean $\bar{y} = 2019.28$) at the recent end.

We emphasize that this recalibration **changes only the score-to-colour mapping $C(z)$ and does not enter the computation of the similarity matrix s_{ij}**, so it leaves every keyword's coordinate x_i, cluster assignment c_i, and link structure unchanged. The recalibrated map is topologically isomorphic to the default map; the two differ only in the visual discriminability of the temporal dimension (Figure 1b).

4.2 Literature search and PRISMA screening (Track B)

Track B assembled the extraction corpus. We searched the Web of Science Core Collection on 5 April 2026 for original research articles published between 2001 and 2025, excluding reviews, book chapters, conference proceedings, and editorial material. Each query combined three dimensions by Boolean logic: ecosystem × driver × biodiversity metric. The ecosystem block matched Track A (*mangrove** joined by OR to the 19 true-mangrove genera). Four driver blocks — climate and extreme weather, pollution, biological invasion, and land-use change (resolved into aquaculture, agriculture, mining and salt pans, and urbanization) — were searched separately. Full strings appear in Supplementary Note 1, Table S3.

The four drivers are climate change and extreme weather, pollution, biological invasion, and land-use change (further resolved into aquaculture, agriculture, mining and salt pans, and urbanization). This classification corresponds to the principal anthropogenic and climatic stressors currently facing mangrove ecosystems: climate change and extreme weather (sea-level rise, storm surge, saline intrusion) reshape the distributional limits and population structure of mangroves by altering tidal inundation duration and salinity gradients; land-use

change (aquaculture ponds, agricultural reclamation, mining and salt pans, urban expansion) is the most direct anthropogenic driver of mangrove area loss and habitat degradation; pollution (heavy metals, microplastics, eutrophication) affects the physiological state and community structure of mangroves and their associated biota by altering sediment and water quality; and biological invasion represents an increasingly recognized biotic stressor that can substantially alter mangrove community composition and ecosystem function. This driver classification accords with the mainstream understanding of the principal pressures on global mangrove change. Friess's synthesis noted that contemporary mangrove dynamics are driven primarily by anthropogenic stressors, including pollution, overextraction, and conversion to aquaculture and agriculture, together with sea-level rise and extreme-weather events intensifying under climate change[13]. We accordingly set these four drivers as the core dimensions of the search framework, so as to systematically cover the principal, well-established ecological stressors in the current literature.

The biodiversity block and the mangrove block were applied identically across all four drivers, fixing the search scope across stressors so that cross-driver differences in yield reflect the literature itself rather than uneven query breadth, and guaranteeing that every effect size — regardless of driver — is drawn from the same response vocabulary, conferring absolute statistical comparability and methodological consistency across stressors. The block deliberately excludes area, extent, and cover: because the study tests whether coarse area-based proxies mask fine-scale change, admitting them into the response block would conflate the response variable with the macro-scale metric under scrutiny.

We screened records under the PRISMA 2020 framework. The four queries identified 10,071 records. Automated filtering on document type and year removed 1,856, leaving 8,215. We then removed 1,471 records — 139 retrieved under more than one driver (cross-driver duplicates) and 1,332 retracted or full-text-unavailable — for a final corpus of 6,744 unique articles. Because one article can match several drivers, the corpus resolves to 6,883 article × driver records (6,744 + 139) (Full PRISMA 2020 flow in Supplementary Note 2, Table S4, Fig. 5.).

4.3 AI-augmented data extraction via retrieval-augmented generation (RAG)

4.3.1 The twin bottlenecks of throughput and audit trail

At the scale of 6,744 unique articles, manual data extraction faces two irreconcilable constraints. The first is a **throughput bottleneck**: full-text adjudication of whether each article contains extractable paired control–impact evidence is the rate-limiting step of the whole workflow, and it accrues reviewer fatigue and criterion drift over time. The second is the **absence of an audit trail**: manual extraction rarely preserves, for each recorded value, a verifiable link from the "database cell" back to the "source page and paragraph," so that once challenged it often cannot be reconstructed value by value. We replaced manual extraction with a retrieval-augmented-generation (RAG) pipeline built on a large language model (Google NotebookLM, backed by the Gemini model family), applying one fixed protocol across all 6,744 articles to decouple extraction consistency from individual reviewers and to generate an auditable evidence anchor for every value.

4.3.2 The RAG computational logic of NotebookLM

When a standard large language model answers a question directly, the answer is generated from its parametric memory, without provenance and prone to hallucination. The core of RAG is to **constrain generation to retrieved source evidence**. For each article d the pipeline performs four steps.

First, **chunking and embedding**. The full text is split into semantically coherent passage chunks $\{c_1, c_2, \ldots, c_m\}$ and mapped by an embedding model to vectors $\mathbf{e}(c_j) \in \mathbb{R}^k$, forming the article's vector index.

Second, **semantic retrieval**. For each target field q (e.g. "control-group mean"), the query vector $\mathbf{e}(q)$ is compared with all chunk vectors by cosine similarity, retrieving the semantically most relevant source passages:

$$\mathrm{Retrieve}(q, d) = \mathrm{Top}_{c_j \in d} \frac{\mathbf{e}(q) \cdot \mathbf{e}(c_j)}{\| \mathbf{e}(q) \| \, \| \mathbf{e}(c_j) \|}.$$

Third, **evidence-anchored generation**. Each value is produced conditioned solely on the retrieved passages, under a fixed prompt protocol that forbids inference beyond the text:

$$\hat{v}_q = \underset{v}{\mathrm{argmax}} \, P(v \mid q, \, \mathrm{Retrieve}(q, d), \, \Pi), \qquad \text{s.t. } v \sqsubseteq \mathrm{Retrieve}(q, d),$$

where Π is the fixed system instruction (§4.3.3) and the constraint $v \sqsubseteq \mathrm{Retrieve}(q, d)$ requires the value to be supportable by the retrieved evidence; where the evidence is

insufficient to support a field, the protocol forces the model to emit an explicit missing-data token (e.g. "Data in Figure X, needs manual extraction") rather than filling in from prior knowledge.

Fourth, **provenance write-back**. Each value $\hat{v}_q$ is output together with its evidence location ℓ_q (table number / page / source sentence), forming a triple $\langle \hat{v}_q, \ell_q, \text{quote}_q \rangle$. Every value in the database thus carries an auditable link back to the source text.

Because a single notebook admits a bounded number of source documents, the 6,744-article corpus was loaded and processed in batches (≈300 articles each) under an identical system protocol Π, so that extraction logic does not drift across batches.

4.3.3 Extraction protocol design: five dimensions and the three-gate "lenient intake, strict exit" architecture

Each of the seven driver domains (climate, pollution, biological invasion, agriculture, aquaculture, mining and salt pans, urbanization) carries a structurally identical system instruction Π that differs only in its exclusion rule and driver lexicon. Each parses every article along **five extraction dimensions**, which are not an arbitrary field list but each serve a specific downstream step:

Dimension 1 — Spatial and metadata (first author, year, DOI, coordinates or precise locality, biogeographic realm). Its purpose is to give each observation a **geographic anchor**, supporting the later spatial validation against the Global Mangrove Watch base layer and the realm-constrained macro-clustering (§4.4); observations lacking coordinates are retained in the database.

Dimension 2 — Stressor profile (sub-category; disturbance mode Pulse/Press), extracted open-endedly, recording verbatim the specific human activity or stressor type in the source rather than forcing it into a preset enumeration. Its purpose is to preserve traceable original labels for cross-driver comparison without losing semantic granularity, and to distinguish pulse (short-term events) from press (long-term pressure) disturbance dynamics.

Dimension 3 — Four-level metric classification (taxon; major class Taxonomic/Functional; sub-class; name; unit; one evidence sentence). This is the **scientific**

core of the protocol: it tags every biological response on both a "taxonomic signal" and a "functional signal" axis, the classificatory basis for the later distinction between taxonomic and functional degradation and for the ecological-scale stratified analysis; rows with no specific biotic receptor are discarded.

Dimension 4 — LnRR basis (control and impact Mean, n, SD/SE, with Table/Page provenance). Its purpose is to **interface directly with effect-size computation**: only with all four ingredients present can a computable log response ratio be formed, and it ensures every effect size carries all the raw quantities and source locations needed for variance estimation.

Dimension 5 — Cross-scale mechanism and teleconnection (scale level; macro socio-economic drivers; degradation-mechanism list with verbatim English quotes). Its purpose is to go beyond the numbers themselves and capture the **macro socio-economic causes behind local ecological decline** (e.g. global supply chains, poverty-driven illegal extraction, coastal urbanization), providing textual evidence for the cross-scale mechanistic interpretation in the Discussion.

These five dimensions are admitted under **differing strictness** — the three-gate "lenient intake, strict exit" architecture:

(1) A biological-exclusivity gate (up-front elimination, Boolean hard constraint). Each instruction opens with an absolute exclusion rule: retain only data points whose measured object is a **living-organism response**, rejecting purely physical, chemical, or engineering quantities (e.g. seawall length, sediment heavy-metal concentration, water salinity, farmed-shrimp yield) unless the authors explicitly tie them to a measured response of a living organism. Formally, for a candidate data point x:

$$\mathrm{Include}(x) = \mathbb{1}[\text{receptor}(x) \in \text{living organisms}] \wedge \mathbb{1}[\exists\ \text{control–impact contrast}(x)].$$

A point failing either condition is skipped before entry. This gate ensures the database retains only population-, community-, and physiological-level biological outcomes.

(2) A labelling gate (lenient intake, non-eliminative). The stressor sub-category, taxon, metric major class (Taxonomic/Functional) and sub-class, ecological scale, and macro socio-economic teleconnection are extracted open-endedly, recording the source's own wording, provisionally tagging ambiguous cases and retaining them (including a later

“Unclassified” bin). The purpose is to maximize retained coverage and to lose no qualifying data point at this stage on account of classification difficulty.

(3) A quantitative-core gate (strict exit, three-way rule). Computing LnRR requires the mean (Mean), sample size (n), and dispersion (SD/SE) for both the control and the impact group. Each candidate observation is handled by the completeness of its quantitative information in one of three ways.

Based on these three rules, **complete records are retained.** Where all six values (control and impact Mean, n, SD/SE) are unambiguously readable from the text, tables, or supplementary material, the observation is entered as a computable effect size. **Wholly absent cases are removed.** Topically relevant articles that report no control–impact quantitative contrast at all (purely descriptive studies, qualitative-only conclusions, or physico-chemical/engineering quantities without a biotic receptor) are judged to contain no qualifying quantitative evidence and yield no observation. The I**ncomplete cases are routed to manual re-check.** Where a data point exists but some element is under-reported or presented only graphically (e.g. a mean shown in a bar chart without its SD, or values residing only in a figure and not precisely readable from the text), the record is flagged rather than discarded (e.g. "Data in Figure X, needs manual extraction"), and a researcher returns to the source figures and tables to verify and complete it — recoverable records are reclaimed as valid effect sizes, and only the genuinely unverifiable are dropped.

This tiered rule, with its provenance constraint (every value tagged to Table/Page and source sentence), both avoids discarding real evidence over a transient gap and ensures that every retained observation is genuinely computable — it is the true sieve behind the 6,744 → 393 reduction.

The three gates together mean that labels are admitted leniently to preserve coverage while the numeric evidence is exited strictly to guarantee every retained observation is real and computable — **this is not data lost in screening but the necessary product of a precision design** (For the complete verbatim prompt template — the unified skeleton and a fully worked example for the Urbanization domain — see Supplementary Note 3.).

4.3.4 The screening funnel: from 6,744 articles to 393 observations

The 6,744 unique articles form a deliberately high-recall topical corpus, admitted on topical

relevance (“mangrove genus ∧ driver ∧ biodiversity term”). But **topical relevance does not imply a computable paired control–impact structure**. The great majority of articles report biodiversity in forms that cannot constitute an effect size — single-site descriptive surveys without a control, remote-sensing and area-mapping studies, modelling and scenario papers, articles mentioning biodiversity only in framing, or those reporting physico-chemical/engineering quantities without a biotic receptor. Applying the three gates **article by article at full-text depth** — the full-text adjudication across all 6,744 articles that is infeasible manually and that the RAG pipeline makes tractable — identified **393 paired control–impact observations** with a qualifying paired structure (the unit of analysis changes from articles to observations here, consistent with the extraction box of Fig. 5). Thereafter, effect-size quality control removed 46 of the 393 (42 with non-positive means for which LnRR is undefined, 3 with context-dependent effect direction, 1 with an unverifiable control), leaving **347** valid effect sizes; spatial-model eligibility screening then removed 4 (1 in non-mangrove habitat, 2 experimental records without coordinates, 1 ecosystem-level receptor), leaving **343** effect sizes entering the spatial multilevel model, traceable to 196 unique articles across 34 biogeographic nodes; the rigorous sensitivity subset is 151(Full effect-size hierarchy and derived ratios in Supplementary Note 4, Table S5.).

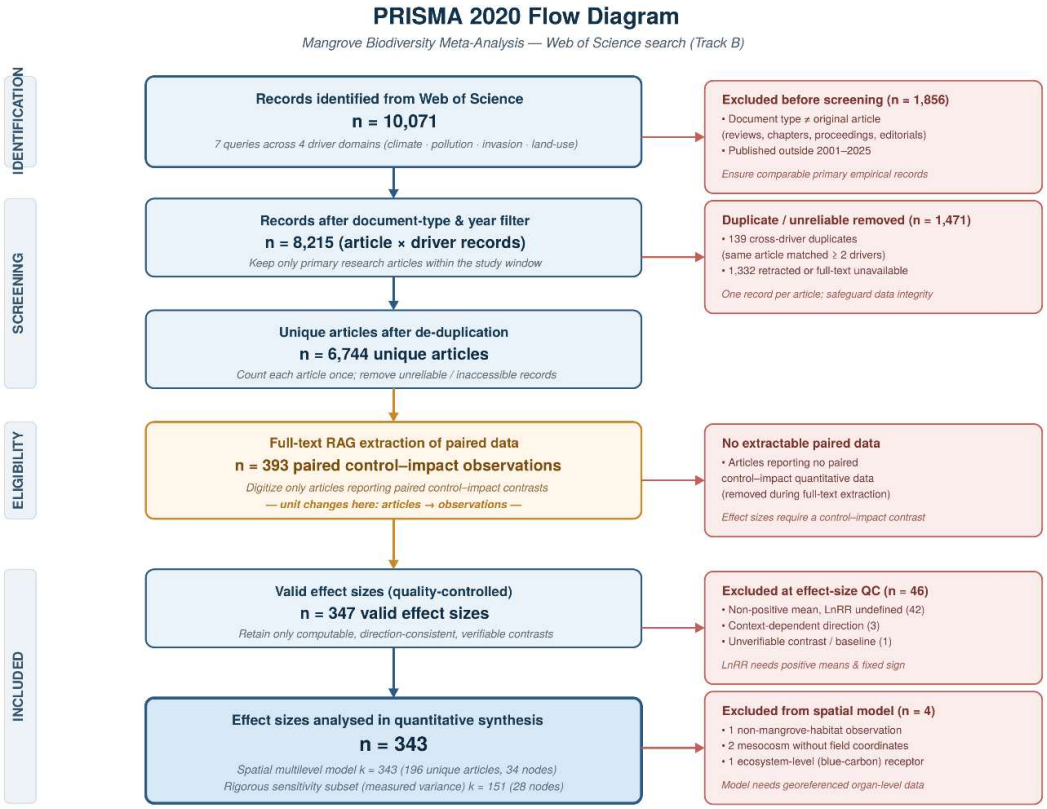
4.3.5 Human-in-the-loop (HITL) validation

To quantify the reliability of the machine extraction, we applied a human-in-the-loop validation protocol. Two researchers (X.W. and J.Y.), blind to the model output, independently re-extracted a random 10% of the corpus. We measured agreement as the **overlap rate between the data entries the two researchers extracted from the same articles** — the proportion of mutually concordant entries — which reached **89%**, on par with expert–expert concordance in comparable syntheses; a senior author (M.G.) adjudicated every non-overlapping entry or classification discrepancy, and this arbitrated consensus served as ground truth and was fed back to refine the prompt protocol Π (sampling and per-driver overlap rates in Supplementary Information).

4.3.6 The pipeline’s role in the study’s overall robustness

This extraction pipeline is not merely an efficiency tool; it provides a threefold foundation for the study’s robustness claims. First, **auditability**: every value is anchored to its source

page, paragraph, and quote, so the evidence chain is fully transparent and verifiable to reviewers rather than a black-box output. Second, **classificatory invariance**: one fixed protocol Π applied across all 6,744 articles means the classification logic does not drift with article order or reviewer state, so the downstream cross-driver, cross-receptor, and cross-scale contrasts reflect differences in the literature itself rather than spurious signals introduced by coding inconsistency. Third, **a foundation for the sensitivity analyses**: precisely because upstream extraction is consistent and traceable, the downstream dual-track ($k = 343$ full / $k = 151$ rigorous) sensitivity analysis and the multilevel Egger and funnel-plot publication-bias diagnostics carry weight — **robustness is not retrofitted at the modelling stage but anchored from the extraction stage**.



Supplementary — records by driver domain (Web of Science, Track B)

Driver domain	Filtered records (RIS)	Final corpus (unique articles)
Climate	2,862	2,388
Pollution	1,817	1,578
Invasion	561	357
Land-use — Agriculture	655	521
Land-use — Aquaculture	458	400
Land-use — Mining & salt-pan	516	425
Land-use — Urbanization	1,346	1,075
Total	**8,215**	**6,744**

Note 1 — Track A (bibliometrics): a parallel search paired the mangrove genus block with the same 12-term biodiversity block, with NO driver terms, retrieving n = 9,097 records. It is used only for publication-trend and VOSviewer keyword-network analyses (Fig. 1) and is not part of this extraction pipeline.
Note 2 — Search executed 5 April 2026, Web of Science Core Collection. Genus names truncated (e.g. Acanthus). The 12-term biodiversity block is identical across all four drivers.*
Note 3 — 6,744 unique articles correspond to 6,883 article × driver records (6,744 + 139 multi-driver matches).
Note 4 — Numbers close along the spine: 10,071 −1,856 → 8,215 −1,471 → 6,744 → [extraction] 393 −46 → 347 −4 → 343. Units switch from articles to observations at extraction.

Figure 5. A transparent, unit-consistent screening funnel converts 10,071 Web of Science records into 343 georeferenced effect sizes for quantitative synthesis. Flow of records through the meta-analysis (Track B) under the PRISMA 2020 framework. The left rail marks the four stages (identification, screening, eligibility, inclusion); the central spine gives the record count retained at each step, and the red boxes give the count and reason for each exclusion. Records were identified from seven Web of Science queries spanning four driver domains (climate, pollution, invasion, and land-use, the last resolved into agriculture, aquaculture, mining & salt-pan, and urbanization). Automated filtering on

document type and publication year (2001–2025) removed 1,856 records; removing 139 cross-driver duplicates and 1,332 retracted or full-text-unavailable records then reduced the corpus to **6,744 unique articles**. The unit of analysis changes at full-text extraction (orange box): articles reporting extractable paired control–impact data were digitized via the retrieval-augmented-generation pipeline into **393 paired observations**, of which 347 passed effect-size quality control (removing non-positive means for which LnRR is undefined, context-dependent effect directions, and unverifiable contrasts) and 343 met the spatial-model eligibility criteria (georeferenced, mangrove-habitat, organ-level receptors). The final synthesis set comprises **k = 343** effect sizes from 196 unique articles across 34 biogeographic nodes, with a rigorous sensitivity subset of k = 151 (28 nodes) restricted to observations with fully measured variance. The parallel bibliometric search (Track A; the mangrove genus block AND the identical 12-term biodiversity block, with no driver terms) retrieved 9,097 records used solely for the publication-trend and VOSviewer keyword-network analyses (Fig. 1) and is not part of this extraction pipeline. Search executed 5 April 2026, Web of Science Core Collection.

4.4 Receptor classification, spatial anchoring, and biogeographic macro-clustering

4.4.1 Receptor framework and inclusion criteria

We categorized effect sizes into four distinct biological receptor classes: flora, invertebrates, vertebrates, and microbiomes. Here, a "receptor" refers to the specific organismal group targeted in a given observation. This scheme allows ecological responses from different studies to be compared across studies by organismal group; accordingly, each observation entering the spatial analysis had to meet two conditions: assignable to one of these four receptors, and carrying a locatable field coordinate.

4.4.2 Record-level geocoding and spatial anchoring

We first assigned a coordinate to every observation and then anchored it to mapped mangrove extent, under a gazetteer-first, manually-adjudicated workflow: most records (313) were geocoded automatically from their study locality against a standard gazetteer, while records the gazetteer could not resolve precisely (e.g. those giving only a bay, estuary, or reserve name) were coordinate-checked and adjudicated by hand with a recorded basis (33), the entire process retained in a per-record geolocation audit (SI;

Node_geocode_audit_v5.csv). Each observation was then anchored to mapped mangrove extent using Global Mangrove Watch v3.0 (Bunting et al., 2022) as the spatial reference layer; this layer is an independent third-party source, not the database we built.

4.4.3 Removal of records that cannot be spatially anchored

We removed two kinds of record: observations falling outside the mangrove polygons, and controlled experiments, which are ecologically informative but lack anchorable field coordinates. Of the 347 QC-passed effect sizes, one lay in non-mangrove habitat; a further three could not enter the receptor-based spatial framework — two mesocosm records without field coordinates, and one record whose observational unit was ecosystem-level carbon stock (blue carbon), retained in the database but incompatible with the four organismal receptors because its unit is an ecosystem function rather than a specific organismal group — yielding **k = 343** georeferenced observations (SI).

4.4.4 Two-tier, realm-constrained macro-clustering

With coordinates anchored, we clustered the 343 sites under a two-tier, realm-constrained scheme. Each site was first assigned to one of the two biogeographically isolated mangrove realms, the Indo-West Pacific (IWP) or the Atlantic–East Pacific (AEP) (Duke et al., 1998; Spalding et al., 2010). Within each realm, sites were grouped by agglomerative hierarchical clustering on the Haversine great-circle distance, using average linkage and a 1,000-km cut-off. Nodes are thus compact by construction and never straddle a realm boundary (maximum within-node distance 1,261 km, at the East Asia / South China Sea node). The data-driven scheme resolved **34 nodes** (IWP 24, AEP 10) — representative nodes include East Asia / South China Sea (spanning Futian–Pearl River Estuary in Shenzhen, Dongzhai Bay on Hainan, and Can Gio in Vietnam) and the Bay of Bengal / eastern India (Sundarbans, Bhitarkanika, Kakinada Bay), together with the northern Gulf of Mexico / South Florida and the Caribbean (e.g. Twin Cays, Belize; Tabasco, Mexico) on the AEP side. These nodes form the top tier of the model's random structure and absorb regional spatial dependence — the primary source of pseudoreplication in a global synthesis (§4.5).

4.4.5 A high-resolution subset within the Indo-West Pacific realm

Beyond the 34 macro-nodes, we built a finer-resolution subset for the IWP realm specifically, for three reasons: IWP is the global centre of mangrove diversity and holds most

of our observations (238 of 343) and nodes (24 of 34); it also carries the densest and most heterogeneous land-use pressure; and under the 1,000-km cut-off the macro-nodes (e.g. the East Asia / South China Sea node, spanning 1,261 km across 40 locations) merge distinct land-use settings and mask within-node contrasts. To resolve the four land-use drivers — agriculture, aquaculture, mining, and urbanization — at a finer grain, we re-aggregated the IWP sites under a stricter distance threshold into 15 high-resolution micro-nodes (carrying 75 land-use observations: mining 27, urbanization 23, agriculture 16, aquaculture 9), used for the spatial depiction of IWP land-use sub-categories in the inset of Figure 4.

4.5 Effect-size quantification and multilevel modelling

4.5.1 Construction of the log response ratio (LnRR) and its rationale

We expressed each biodiversity response as a log response ratio:

$$\mathrm{LnRR} = M \cdot \ln\left(\frac{\bar{X}_I}{\bar{X}_C}\right),$$

where $\bar{X}_I$ and $\bar{X}_C$ are the impact-group and control-group means. We chose the log response ratio over an absolute difference for three reasons: it is a **unit-free** proportional measure, letting responses from different metrics and units (e.g. ind./m², %, mg/kg) be pooled on one scale; the logarithm symmetrizes fold-increases and fold-decreases (a doubling and a halving are equidistant on the log scale), so positive changes are not systematically over-weighted; and it is the established standard quantity in ecological meta-analysis, facilitating comparison with existing literature.

The role of the direction multiplier M is to calibrate sign to ecological meaning. “An increase” carries opposite ecological polarity for different metrics: an increase in richness, biomass, or carbon capacity is beneficial, whereas an increase in mortality, contaminant load, or stress markers is harmful. Pooling them without correction would cancel their signs. We therefore set M **once, at the metric level**: $M = +1$ for beneficial metrics, $M = -1$ for harmful metrics. After this calibration, **a negative LnRR always denotes ecological degradation**, with a uniform and explicit ecological interpretation of sign across the whole database. The ratio is undefined for non-positive means, and such observations were dropped rather than rescued with an artificial offset constant — adding an offset would distort

the proportional relationship and introduce arbitrariness dependent on the constant's value.

4.5.2 Sampling-variance estimation and missing-data imputation

Each effect size's sampling variance was estimated by the delta method (Hedges, Gurevitch & Curtis, 1999) from the two groups' means, dispersion (SD), and sample sizes (n), the basis for subsequent weighting and uncertainty quantification. **The problem** is that primary studies frequently omit SD or n; discarding them wholesale would markedly erode the database's spatial and taxonomic coverage (especially losing small-sample, peripheral-region studies). We therefore imputed on principle: missing SD was reconstructed from the **median coefficient of variation (CV) of complete records of the same metric** — the median rather than the mean, being more robust to outliers — and missing n from the complete-record median, defaulting to $n = 3$, the field-ecology triplicate convention. **Every imputed value is flagged** for tracking and sensitivity analysis.

Imputation preserves coverage but raises a question that must be answered: **could the conclusion be "manufactured" by imputation?** To test this we ran **two parallel data tracks**: a full track ($k = 343$) using all georeferenced effect sizes with imputation, and a rigorous track ($k = 151$) retaining only observations with **measured** SD and n on both the control and impact sides. If the two tracks agree in effect direction and significance, the conclusion is shown not to depend on imputation — **concordance between the tracks is this study's primary robustness criterion**.

4.5.3 The multilevel model: what it does, what it answers, and why specified this way

Both data tracks were fitted with metafor's rma.mv function under restricted maximum likelihood (REML) as multilevel meta-analytic models (Viechtbauer, 2010), to estimate each moderator's pooled effect on the mangrove ecological response (LnRR) and its uncertainty, and to test whether these effects are significant.

Why not an ordinary (single-level) meta-analysis? Because the effect sizes are structurally non-independent: one study typically contributes several observations, and several studies cluster in the same geographic region. Ignoring this nested structure and treating all observations as independent would artificially underestimate standard errors and inflate statistical significance — the **pseudoreplication** problem, especially acute in a

global-scale synthesis. To absorb this non-independence, we used a three-level nested random-effects structure:

$$\sim 1 \mid \text{Node_ID} / \text{Spatial_Meta_Raw} / \text{Obs_ID},$$

partitioning total variance across the regional node (Node_ID), the study (Spatial_Meta_Raw), and the individual observation (Obs_ID). This hierarchical baseline strips spatial- and study-level non-independence and prevents the variance deflation that drives pseudoreplication. **The empirical variance partition confirms the necessity of this specification**: the node level carries only about 1–3% of the variance, whereas the study level (about 54–56%) and observation level (about 43–44%) together carry almost all of it — the real variation lies within and among studies, not among regions, which is precisely why a multilevel rather than fixed-effect synthesis is required(Full variance components and omnibus moderator tests for all four models in Supplementary Note 5, Tables S6–S7.).

On this structure, we assessed each moderator's overall effect with the omnibus Q_M statistic — driver, biological receptor, ecological scale, and the driver × receptor interaction — and quantified unexplained residual heterogeneity with Q_E. All inference used study-clustered robust variance estimation (Huber–White CR1 sandwich estimator, clustered on study; 189 clusters in the full track) to further guard against residual within-study non-independence. The CR2 bias-reduced estimator could not be applied because it is undefined for the three-level random structure used here; with 189 clusters the two estimators are expected to differ negligibly. (Full coefficients in Supplementary Note 5, §5.2–5.5, Tables S8–S11.).

Because a non-significant contrast establishes only a failure to detect a difference and not the absence of one, we tested the scale-invariance and metric-class results directly using two one-sided tests (TOST). For each contrast we declared equivalence when the 90% confidence interval fell entirely within ±Δ, reporting p_TOST as the larger of the two one-sided p-values. The equivalence bound was set a priori at Δ = 0.57 LnRR units — the magnitude of the pooled degradation effect — on the reasoning that two scales tell a materially different story only if they differ by as much as the average effect itself. To keep the conclusion independent of that choice we additionally report, for every contrast, the smallest bound at which equivalence holds (Δ_min, the outer edge of the 90% interval) and

a sensitivity sweep across $\Delta \in [0.15, 0.60]$. Every contrast was classified as equivalent, different, trivially different, or inconclusive; inconclusive outcomes are reported as such (Supplementary Note 5, §5.8).

4.5.4 Publication-bias diagnostics

Journals and authors both favour studies with "significant results": a paper concluding that "pollution significantly reduces mangrove biodiversity" is easily published, whereas one finding "no detectable effect" is often shelved. We must therefore answer a pointed challenge — **could the cross-scale-consistent negative degradation conclusion arise merely because we captured only papers reporting negative results?** The judgement rests on a statistical intuition: large, high-precision studies are published regardless of whether the result is significant, so their effect sizes should scatter symmetrically around the true value; whereas small, low-precision studies, if only those with "large effects" are published, produce a systematic "smaller sample, larger effect" association. Plotting effect against precision yields a symmetric funnel (funnel plot) if unbiased, and a missing corner at the funnel's base (the low-precision side) if biased (Fig. S2, S3.); Egger regression quantifies this asymmetry by a statistical test.

We tested publication bias with multilevel Egger regression and funnel plots. **Note a pitfall specific to LnRR**: its sampling variance is derived from the group means and is therefore mathematically correlated with the effect size itself; using the standard error as a predictor can detect spurious funnel asymmetry even when no true bias exists. To avoid this, we used an **effective-sample-size**-based precision term as the primary test statistic —

$$n_{\text{eff}} = \frac{n_C\, n_I}{n_C + n_I},$$

which depends only on sample sizes, not on the group means, thereby avoiding the mechanical correlation above (Nakagawa et al., 2022), and we report the bias-corrected pooled effect (Full Egger and time-lag regression results in Supplementary Note 6, Table S15.). Because trim-and-fill has no established theoretical definition under a three-level nested random-effects structure, it was not applied.

4.5.5 Results of the robustness checks

Three lines of evidence jointly support the robustness of the core conclusion. **First, dual-**

track concordance: the main effects agree closely between the full track ($k = 343$) and the rigorous track ($k = 151$) — the climate, land-use, and pollution drivers, the flora, invertebrate, and vertebrate receptors, and all four ecological scales are concordant in direction and significance across tracks, with only the normal drop in significance level as the sample narrows, indicating the result is not an imputation artefact (only the microbiome receptor shows sensitivity — significant in the full track, non-significant in the rigorous track — and is treated cautiously in the main text; the core conclusions do not depend on it). **Second, no detectable publication bias:** the primary effective-sample-size Egger test is non-significant in both tracks (full $p = 0.307$; rigorous $p = 0.872$), detecting no funnel asymmetry; the time-lag test is likewise non-significant, so effect magnitude does not drift with publication year. **Third, the conclusion is unchanged after bias correction:** even under the most conservative correction, the pooled intercept remains significantly negative (about −0.43 to −0.60), of the same order as the uncorrected pooled estimate (about −0.57). Taken together, the significant cross-driver, cross-receptor, cross-scale negative degradation of mangrove biodiversity is neither an artefact of variance imputation nor a product of publication bias. Full coefficients, variance components, and bias diagnostics appear in Supplementary Notes 5–7 (Tables S6–S15; Figs. S2–S3).

4.5.6 Computing environment and reproducibility

Deterministic processing — parsing, effect-size computation, variance estimation, and spatial clustering — ran in Python 3.11.7 (pandas 2.3.3, NumPy 1.26.4, scikit-learn 1.5.2); model fitting and plotting ran in R 4.5.1 (metafor 5.0.1, orchaRd 2.2.0). The analysis-ready database, value-level provenance log, and all code are available in the project repository.

Non-significance in the pairwise scale contrasts (§4.5.3) and the metric-class contrast establishes only that the data do not resolve a difference, not that the compared groups respond alike. We therefore tested both claims with two one-sided tests (TOST), which invert the null hypothesis to "the groups differ by at least Δ." Equivalence at bound Δ is declared when the 90% confidence interval of a contrast lies entirely within (−Δ, +Δ). We fixed the primary bound at Δ = 0.57, the midpoint of the −0.49 to −0.65 range spanned by the four scale-level marginal means, before running any test, and report a full sensitivity sweep (Δ = 0.15–0.60) together with the bound-free statistic Δ_min (the smallest Δ at which equivalence

holds) for every contrast. Inference used cluster-robust (Huber–White CR1) standard errors clustered on study, referred to a t-distribution; the small-sample CR2 correction was not used, because clubSandwich cannot return a CR2 covariance matrix for this three-level nested random structure. Each contrast received one of four verdicts — Equivalent, Inconclusive, Trivially different, or Different — from the uncorrected p_TOST, itself an intersection-union test requiring no multiplicity correction; Holm-adjusted p_TOST is reported alongside as a conservative secondary check.

References

1 Cerri, F., Mohamed, S. & Galli, P. Mangrove forests as a natural trap for marine plastic litter: Insights from the Maldives. *Mar Pollut Bull* **213**, 117677 (2025). https://doi.org/10.1016/j.marpolbul.2025.117677

2 Fell, A., Jagadesh, S., Duthie, A. B., Kirkpatrick, L. & Bunnefeld, N. Global evidence synthesis on land-use change and zoonotic risks. *Nature Sustainability* **9**, 142-152 (2026). https://doi.org/10.1038/s41893-025-01750-2

3 Zhang, Z., Murray, N. J., Song, X.-P., Bunting, P., Worthington, T. A., Fatoyinbo, L., Mao, D., Jia, M., Arifanti, V. B., Aung, T., San Htay, S. & Friess, D. A. Unexpected expansion and regrowth in Earth's mangrove forests over the past four decades. *Science* **392**, 1082-1087 (2026). https://doi.org/10.1126/science.aec9773

4 Palacios, O. A., Adame-Gallegos, J. R., Rivera-Chavira, B. E. & Nevarez-Moorillon, G. V. Antibiotics, Multidrug-Resistant Bacteria, and Antibiotic Resistance Genes: Indicators of Contamination in Mangroves? *Antibiotics (Basel)* **10** (2021). https://doi.org/10.3390/antibiotics10091103

5 Sievers, M., Brown, C. J., McGowan, J., Turschwell, M. P., Buelow, C. A., Holgate, B., Pearson, R. M., Adame, M. F., Andradi-Brown, D. A., Arnell, A., Mackey, B. G., Ermgassen, P., Gosling, J., McOwen, C. J., Worthington, T. A. & Connolly, R. M. Co-occurrence of biodiversity, carbon storage, coastal protection, and fish and invertebrate production to inform global mangrove conservation planning. *Sci Total Environ* **904**, 166357 (2023). https://doi.org/10.1016/j.scitotenv.2023.166357

6 Anwar, R., Lihawa, F., Baderan, D. W. K., Mahmud, M., Olii, A. H. & Hasim. Mangrove in Biodiversitas: A Systematic Review of Biodiversity, Blue Carbon, and Ecosystem Services in Southeast Asia (2020-2025). *International Journal of Research and Review* (2020). https://doi.org/10.52403/ijrr.20260106

7 Blythe, J. L., Claudet, J., Gill, D., Ban, N. C., Epstein, G., Gurney, G. G., Jupiter, S. D., Mahajan, S. L., Mangubhai, S., Turner, R., Bennett, N. J., D'Agata, S., Franks, P., Lau, J., Ahmadia, G., Andrachuk, M., Annasawmy, P., Brun, V., Darling, E. S., Di Franco, A., Evans, L., Lazzari, N., Naggea, J., Relano, V., Pertuz, M. C., Villasante, S. & Zafra-Calvo, N. The Ocean Equity Index. *Nature* **650**, 123-128 (2026). https://doi.org/10.1038/s41586-025-09976-y

8 Elwin, A., Robinson, E. J. Z., Feola, G., Jintana, V. & Clark, J. How is mangrove ecosystem health defined? A local community perspective from coastal Thailand. *Ocean & Coastal Management* **251** (2024). https://doi.org/10.1016/j.ocecoaman.2024.107037

9 Keck, F., Peller, T., Alther, R., Barouillet, C., Blackman, R., Capo, E., Chonova, T., Couton, M., Fehlinger, L., Kirschner, D., Knusel, M., Muneret, L., Oester, R., Tapolczai, K., Zhang, H. & Altermatt, F. The global human impact on biodiversity. *Nature* **641**, 395-400 (2025). https://doi.org/10.1038/s41586-025-08752-2

10 Heck, N., Goldberg, L., Andradi-Brown, D. A., Campbell, A., Narayan, S., Ahmadia, G. N. & Lagomasino, D. Global drivers of mangrove loss in protected areas. *Conserv Biol* **38**, e14293 (2024). https://doi.org/10.1111/cobi.14293

11 Prütz, R., Rogelj, J., Ganti, G., Price, J., Warren, R., Forstenhäusler, N., Wu, Y., Augustynczik, A. L. D., Wögerer, M., Krisztin, T., Havlík, P., Kraxner, F., Frank, S., Hasegawa, T., Doelman, J. C.,

Daioglou, V., Humpenöder, F., Popp, A. & Fuss, S. Biodiversity implications of land-intensive carbon dioxide removal. *Nature Climate Change* **16**, 155-163 (2026). https://doi.org/10.1038/s41558-026-02557-5

12 Feller, I. C., Lovelock, C. E., Berger, U., McKee, K. L., Joye, S. B. & Ball, M. C. Biocomplexity in Mangrove Ecosystems. *Annual Review of Marine Science* **2**, 395-417 (2010). https://doi.org/https://doi.org/10.1146/annurev.marine.010908.163809

13 Friess, D. A., Rogers, K., Lovelock, C. E., Krauss, K. W., Hamilton, S. E., Lee, S. Y., Lucas, R., Primavera, J., Rajkaran, A. & Shi, S. The State of the World's Mangrove Forests: Past, Present, and Future. *Annual Review of Environment and Resources* **44**, 89-115 (2019). https://doi.org/https://doi.org/10.1146/annurev-environ-101718-033302

14 Bunting, P., Rosenqvist, A., Lucas, R. M., Rebelo, L.-M., Hilarides, L., Thomas, N., Hardy, A., Itoh, T., Shimada, M. & Finlayson, C. M. The Global Mangrove Watch—A New 2010 Global Baseline of Mangrove Extent. *Remote Sensing* **10**, 1669 (2018).

15 Goldberg, L., Lagomasino, D., Thomas, N. & Fatoyinbo, T. Global declines in human-driven mangrove loss. *Global Change Biology* **26**, 5844-5855 (2020). https://doi.org/https://doi.org/10.1111/gcb.15275

16 Aarif, K. M., Rubeena, K. A., Nefla, A., Musilova, Z., Musil, P. & Bin Muzaffar, S. Bio-concentration of hazardous metals in migrant shorebirds in a key conservation reserve and adjoining areas on the west coast of India. *Ecotoxicol Environ Saf* **289**, 117690 (2025). https://doi.org/10.1016/j.ecoenv.2025.117690

17 Hudson, L. N., Newbold, T., Contu, S., Hill, S. L. L., Lysenko, I., De Palma, A., Phillips, H. R. P., Senior, R. A., Bennett, D. J., Booth, H., Choimes, A., Correia, D. L. P., Day, J., Echeverría-Londoño, S., Garon, M., Harrison, M. L. K., Ingram, D. J., Jung, M., Kemp, V., Kirkpatrick, L., Martin, C. D., Pan, Y., White, H. J., Aben, J., Abrahamczyk, S., Adum, G. B., Aguilar-Barquero, V., Aizen, M. A., Ancrenaz, M., Arbeláez-Cortés, E., Armbrecht, I., Azhar, B., Azpiroz, A. B., Baeten, L., Báldi, A., Banks, J. E., Barlow, J., Batáry, P., Bates, A. J., Bayne, E. M., Beja, P., Berg, Å., Berry, N. J., Bicknell, J. E., Bihn, J. H., Böhning-Gaese, K., Boekhout, T., Boutin, C., Bouyer, J., Brearley, F. Q., Brito, I., Brunet, J., Buczkowski, G., Buscardo, E., Cabra-García, J., Calviño-Cancela, M., Cameron, S. A., Cancello, E. M., Carrijo, T. F., Carvalho, A. L., Castro, H., Castro-Luna, A. A., Cerda, R., Cerezo, A., Chauvat, M., Clarke, F. M., Cleary, D. F. R., Connop, S. P., D'Aniello, B., da Silva, P. G., Darvill, B., Dauber, J., Dejean, A., Diekötter, T., Dominguez-Haydar, Y., Dormann, C. F., Dumont, B., Dures, S. G., Dynesius, M., Edenius, L., Elek, Z., Entling, M. H., Farwig, N., Fayle, T. M., Felicioli, A., Felton, A. M., Ficetola, G. F., Filgueiras, B. K. C., Fonte, S. J., Fraser, L. H., Fukuda, D., Furlani, D., Ganzhorn, J. U., Garden, J. G., Gheler-Costa, C., Giordani, P., Giordano, S., Gottschalk, M. S., Goulson, D., Gove, A. D., Grogan, J., Hanley, M. E., Hanson, T., Hashim, N. R., Hawes, J. E., Hébert, C., Helden, A. J., Henden, J.-A., Hernández, L., Herzog, F., Higuera-Diaz, D., Hilje, B., Horgan, F. G., Horváth, R., Hylander, K., Isaacs-Cubides, P., Ishitani, M., Jacobs, C. T., Jaramillo, V. J., Jauker, B., Jonsell, M., Jung, T. S., Kapoor, V., Kati, V., Katovai, E., Kessler, M., Knop, E., Kolb, A., Kőrösi, Á., Lachat, T., Lantschner, V., Le Féon, V., LeBuhn, G., Légaré, J.-P., Letcher, S. G., Littlewood, N. A., López-Quintero, C. A., Louhaichi, M., Lövei, G. L., Lucas-Borja, M. E., Luja, V. H., Maeto, K., Magura, T., Mallari, N. A., Marin-Spiotta, E., Marshall, E. J. P., Martínez, E., Mayfield, M. M., Mikusinski, G., Milder, J. C., Miller, J. R., Morales, C. L., Muchane, M. N., Muchane, M., Naidoo, R., Nakamura, A., Naoe, S., Nates-Parra, G., Navarrete Gutierrez, D. A., Neuschulz, E. L., Noreika, N., Norfolk, O., Noriega, J. A., Nöske, N. M., O'Dea, N., Oduro, W., Ofori-Boateng, C., Oke, C. O., Osgathorpe, L.

M., Paritsis, J., Parra-H, A., Pelegrin, N., Peres, C. A., Persson, A. S., Petanidou, T., Phalan, B., Philips, T. K., Poveda, K., Power, E. F., Presley, S. J., Proença, V., Quaranta, M., Quintero, C., Redpath-Downing, N. A., Reid, J. L., Reis, Y. T., Ribeiro, D. B., Richardson, B. A., Richardson, M. J., Robles, C. A., Römbke, J., Romero-Duque, L. P., Rosselli, L., Rossiter, S. J., Roulston, T. a. H., Rousseau, L., Sadler, J. P., Sáfián, S., Saldaña-Vázquez, R. A., Samnegård, U., Schüepp, C., Schweiger, O., Sedlock, J. L., Shahabuddin, G., Sheil, D., Silva, F. A. B., Slade, E. M., Smith-Pardo, A. H., Sodhi, N. S., Somarriba, E. J., Sosa, R. A., Stout, J. C., Struebig, M. J., Sung, Y.-H., Threlfall, C. G., Tonietto, R., Tóthmérész, B., Tscharntke, T., Turner, E. C., Tylianakis, J. M., Vanbergen, A. J., Vassilev, K., Verboven, H. A. F., Vergara, C. H., Vergara, P. M., Verhulst, J., Walker, T. R., Wang, Y., Watling, J. I., Wells, K., Williams, C. D., Willig, M. R., Woinarski, J. C. Z., Wolf, J. H. D., Woodcock, B. A., Yu, D. W., Zaitsev, A. S., Collen, B., Ewers, R. M., Mace, G. M., Purves, D. W., Scharlemann, J. P. W. & Purvis, A. The PREDICTS database: a global database of how local terrestrial biodiversity responds to human impacts. *Ecology and Evolution* **4**, 4701-4735 (2014). https://doi.org/https://doi.org/10.1002/ece3.1303

18 Dornelas, M., Antão, L. H., Moyes, F., Bates, A. E., Magurran, A. E., Adam, D., Akhmetzhanova, A. A., Appeltans, W., Arcos, J. M., Arnold, H., Ayyappan, N., Badihi, G., Baird, A. H., Barbosa, M., Barreto, T. E., Bässler, C., Bellgrove, A., Belmaker, J., Benedetti-Cecchi, L., Bett, B. J., Bjorkman, A. D., Błażewicz, M., Blowes, S. A., Bloch, C. P., Bonebrake, T. C., Boyd, S., Bradford, M., Brooks, A. J., Brown, J. H., Bruelheide, H., Budy, P., Carvalho, F., Castañeda-Moya, E., Chen, C. A., Chamblee, J. F., Chase, T. J., Siegwart Collier, L., Collinge, S. K., Condit, R., Cooper, E. J., Cornelissen, J. H. C., Cotano, U., Kyle Crow, S., Damasceno, G., Davies, C. H., Davis, R. A., Day, F. P., Degraer, S., Doherty, T. S., Dunn, T. E., Durigan, G., Duffy, J. E., Edelist, D., Edgar, G. J., Elahi, R., Elmendorf, S. C., Enemar, A., Ernest, S. K. M., Escribano, R., Estiarte, M., Evans, B. S., Fan, T.-Y., Turini Farah, F., Loureiro Fernandes, L., Farneda, F. Z., Fidelis, A., Fitt, R., Fosaa, A. M., Daher Correa Franco, G. A., Frank, G. E., Fraser, W. R., García, H., Cazzolla Gatti, R., Givan, O., Gorgone-Barbosa, E., Gould, W. A., Gries, C., Grossman, G. D., Gutierréz, J. R., Hale, S., Harmon, M. E., Harte, J., Haskins, G., Henshaw, D. L., Hermanutz, L., Hidalgo, P., Higuchi, P., Hoey, A., Van Hoey, G., Hofgaard, A., Holeck, K., Hollister, R. D., Holmes, R., Hoogenboom, M., Hsieh, C.-h., Hubbell, S. P., Huettmann, F., Huffard, C. L., Hurlbert, A. H., Macedo Ivanauskas, N., Janík, D., Jandt, U., Jażdżewska, A., Johannessen, T., Johnstone, J., Jones, J., Jones, F. A. M., Kang, J., Kartawijaya, T., Keeley, E. C., Kelt, D. A., Kinnear, R., Klanderud, K., Knutsen, H., Koenig, C. C., Kortz, A. R., Král, K., Kuhnz, L. A., Kuo, C.-Y., Kushner, D. J., Laguionie-Marchais, C., Lancaster, L. T., Min Lee, C., Lefcheck, J. S., Lévesque, E., Lightfoot, D., Lloret, F., Lloyd, J. D., López-Baucells, A., Louzao, M., Madin, J. S., Magnússon, B., Malamud, S., Matthews, I., McFarland, K. P., McGill, B., McKnight, D., McLarney, W. O., Meador, J., Meserve, P. L., Metcalfe, D. J., Meyer, C. F. J., Michelsen, A., Milchakova, N., Moens, T., Moland, E., Moore, J., Mathias Moreira, C., Müller, J., Murphy, G., Myers-Smith, I. H., Myster, R. W., Naumov, A., Neat, F., Nelson, J. A., Paul Nelson, M., Newton, S. F., Norden, N., Oliver, J. C., Olsen, E. M., Onipchenko, V. G., Pabis, K., Pabst, R. J., Paquette, A., Pardede, S., Paterson, D. M., Pélissier, R., Peñuelas, J., Pérez-Matus, A., Pizarro, O., Pomati, F., Post, E., Prins, H. H. T., Priscu, J. C., Provoost, P., Prudic, K. L., Pulliainen, E., Ramesh, B. R., Mendivil Ramos, O., Rassweiler, A., Rebelo, J. E., Reed, D. C., Reich, P. B., Remillard, S. M., Richardson, A. J., Richardson, J. P., van Rijn, I., Rocha, R., Rivera-Monroy, V. H., Rixen, C., Robinson, K. P., Ribeiro Rodrigues, R., de Cerqueira Rossa-Feres, D., Rudstam, L., Ruhl, H., Ruz, C. S., Sampaio, E. M., Rybicki, N., Rypel, A., Sal, S., Salgado, B., Santos, F. A. M., Savassi-Coutinho, A. P., Scanga, S., Schmidt, J., Schooley, R.,

Setiawan, F., Shao, K.-T., Shaver, G. R., Sherman, S., Sherry, T. W., Siciński, J., Sievers, C., da Silva, A. C., Rodrigues da Silva, F., Silveira, F. L., Slingsby, J., Smart, T., Snell, S. J., Soudzilovskaia, N. A., Souza, G. B. G., Maluf Souza, F., Castro Souza, V., Stallings, C. D., Stanforth, R., Stanley, E. H., Mauro Sterza, J., Stevens, M., Stuart-Smith, R., Rondon Suarez, Y., Supp, S., Yoshio Tamashiro, J., Tarigan, S., Thiede, G. P., Thorn, S., Tolvanen, A., Teresa Zugliani Toniato, M., Totland, Ø., Twilley, R. R., Vaitkus, G., Valdivia, N., Vallejo, M. I., Valone, T. J., Van Colen, C., Vanaverbeke, J., Venturoli, F., Verheye, H. M., Vianna, M., Vieira, R. P., Vrška, T., Quang Vu, C., Van Vu, L., Waide, R. B., Waldock, C., Watts, D., Webb, S., Wesołowski, T., White, E. P., Widdicombe, C. E., Wilgers, D., Williams, R., Williams, S. B., Williamson, M., Willig, M. R., Willis, T. J., Wipf, S., Woods, K. D., Woehler, E. J., Zawada, K. & Zettler, M. L. BioTIME: A database of biodiversity time series for the Anthropocene. *Global Ecology and Biogeography* **27**, 760-786 (2018). https://doi.org/https://doi.org/10.1111/geb.12729

19 McRae, L., Deinet, S. & Freeman, R. The Diversity-Weighted Living Planet Index: Controlling for Taxonomic Bias in a Global Biodiversity Indicator. *PLOS ONE* **12**, e0169156 (2017). https://doi.org/10.1371/journal.pone.0169156

20 Schipper, A. M., Hilbers, J. P., Meijer, J. R., Antão, L. H., Benítez-López, A., de Jonge, M. M. J., Leemans, L. H., Scheper, E., Alkemade, R., Doelman, J. C., Mylius, S., Stehfest, E., van Vuuren, D. P., van Zeist, W.-J. & Huijbregts, M. A. J. Projecting terrestrial biodiversity intactness with GLOBIO 4. *Global Change Biology* **26**, 760-771 (2020). https://doi.org/https://doi.org/10.1111/gcb.14848

21 Macreadie, P. I., Anton, A., Raven, J. A., Beaumont, N., Connolly, R. M., Friess, D. A., Kelleway, J. J., Kennedy, H., Kuwae, T., Lavery, P. S., Lovelock, C. E., Smale, D. A., Apostolaki, E. T., Atwood, T. B., Baldock, J., Bianchi, T. S., Chmura, G. L., Eyre, B. D., Fourqurean, J. W., Hall-Spencer, J. M., Huxham, M., Hendriks, I. E., Krause-Jensen, D., Laffoley, D., Luisetti, T., Marbà, N., Masque, P., McGlathery, K. J., Megonigal, J. P., Murdiyarso, D., Russell, B. D., Santos, R., Serrano, O., Silliman, B. R., Watanabe, K. & Duarte, C. M. The future of Blue Carbon science. *Nature Communications* **10**, 3998 (2019). https://doi.org/10.1038/s41467-019-11693-w

22 Zhang, Y., Huang, G., Wang, W., Chen, L. & Lin, G. Interactions between mangroves and exotic Spartina in an anthropogenically disturbed estuary in southern China. *Ecology* **93**, 588-597 (2012). https://doi.org/10.1890/11-1302.1

23 Bayen, S. Occurrence, bioavailability and toxic effects of trace metals and organic contaminants in mangrove ecosystems: a review. *Environ Int* **48**, 84-101 (2012). https://doi.org/10.1016/j.envint.2012.07.008

24 Armour, K. C. Energy budget constraints on climate sensitivity in light of inconstant climate feedbacks. *Nature Climate Change* **7**, 331-335 (2017). https://doi.org/10.1038/nclimate3278

25 Kuussaari, M., Bommarco, R., Heikkinen, R. K., Helm, A., Krauss, J., Lindborg, R., Öckinger, E., Pärtel, M., Pino, J., Rodà, F., Stefanescu, C., Teder, T., Zobel, M. & Steffan-Dewenter, I. Extinction debt: a challenge for biodiversity conservation. *Trends in Ecology & Evolution* **24**, 564-571 (2009). https://doi.org/https://doi.org/10.1016/j.tree.2009.04.011

26 Mouillot, D., Bellwood, D. R., Baraloto, C., Chave, J., Galzin, R., Harmelin-Vivien, M., Kulbicki, M., Lavergne, S., Lavorel, S., Mouquet, N., Paine, C. E. T., Renaud, J. & Thuiller, W. Rare Species Support Vulnerable Functions in High-Diversity Ecosystems. *PLOS Biology* **11**, e1001569 (2013). https://doi.org/10.1371/journal.pbio.1001569

27 Loisel, J., Gallego-Sala, A. V., Amesbury, M. J., Magnan, G., Anshari, G., Beilman, D. W., Benavides,

J. C., Blewett, J., Camill, P., Charman, D. J., Chawchai, S., Hedgpeth, A., Kleinen, T., Korhola, A., Large, D., Mansilla, C. A., Müller, J., van Bellen, S., West, J. B., Yu, Z., Bubier, J. L., Garneau, M., Moore, T., Sannel, A. B. K., Page, S., Väliranta, M., Bechtold, M., Brovkin, V., Cole, L. E. S., Chanton, J. P., Christensen, T. R., Davies, M. A., De Vleeschouwer, F., Finkelstein, S. A., Frolking, S., Gałka, M., Gandois, L., Girkin, N., Harris, L. I., Heinemeyer, A., Hoyt, A. M., Jones, M. C., Joos, F., Juutinen, S., Kaiser, K., Lacourse, T., Lamentowicz, M., Larmola, T., Leifeld, J., Lohila, A., Milner, A. M., Minkkinen, K., Moss, P., Naafs, B. D. A., Nichols, J., O'Donnell, J., Payne, R., Philben, M., Piilo, S., Quillet, A., Ratnayake, A. S., Roland, T. P., Sjögersten, S., Sonnentag, O., Swindles, G. T., Swinnen, W., Talbot, J., Treat, C., Valach, A. C. & Wu, J. Expert assessment of future vulnerability of the global peatland carbon sink. *Nature Climate Change* **11**, 70-77 (2021). https://doi.org/10.1038/s41558-020-00944-0

28 Aguilos, M., Sun, G., Bulluck, J., Shi, M., Han, X., Carter, C., Brannum, K., Middlebrough, B., Watts, J., Webb, J., Whitley, M., Ganjam, M., Liu, N., Baniya, B., Mitra, B., Prajapati, P., Minick, K., McNulty, S., Noormets, A. & King, J. Tree mortality provides early warning sign of ecosystem functional transition in coastal freshwater forested wetlands. *Environmental Research Letters* **20** (2025). https://doi.org/10.1088/1748-9326/ae0057

29 Richardson, L. E., Graham, N. A. J., Pratchett, M. S., Eurich, J. G. & Hoey, A. S. Mass coral bleaching causes biotic homogenization of reef fish assemblages. *Glob Chang Biol* **24**, 3117-3129 (2018). https://doi.org/10.1111/gcb.14119

30 Callaghan, M., Schleussner, C.-F., Nath, S., Lejeune, Q., Knutson, T. R., Reichstein, M., Hansen, G., Theokritoff, E., Andrijevic, M., Brecha, R. J., Hegarty, M., Jones, C., Lee, K., Lucas, A., van Maanen, N., Menke, I., Pfleiderer, P., Yesil, B. & Minx, J. C. Machine-learning-based evidence and attribution mapping of 100,000 climate impact studies. *Nature Climate Change* **11**, 966-972 (2021). https://doi.org/10.1038/s41558-021-01168-6

31 Gurevitch, J., Koricheva, J., Nakagawa, S. & Stewart, G. Meta-analysis and the science of research synthesis. *Nature* **555**, 175-182 (2018). https://doi.org/10.1038/nature25753

32 Westgate, M. J., Haddaway, N. R., Cheng, S. H., McIntosh, E. J., Marshall, C. & Lindenmayer, D. B. Software support for environmental evidence synthesis. *Nature Ecology & Evolution* **2**, 588-590 (2018). https://doi.org/10.1038/s41559-018-0502-x

33 Vazquez-Rosas-Landa, M., Perez-Ceballos, R., Zaldivar-Jimenez, A., Hereira, S., Perez Gonzalez, L., Prieto-Davo, A., Celis-Hernandez, O. & Canales-Delgadillo, J. C. Impact of seasonal flooding and hydrological connectivity loss on microbial community dynamics in mangrove sediments of the southern Gulf of Mexico. *PeerJ* **13**, e19371 (2025). https://doi.org/10.7717/peerj.19371

34 Twomey, A. J., Nunez, K., Carr, J. A., Crooks, S., Friess, D. A., Glamore, W., Orr, M., Reef, R., Rogers, K., Waltham, N. J. & Lovelock, C. E. Planning hydrological restoration of coastal wetlands: Key model considerations and solutions. *Sci Total Environ* **915**, 169881 (2024). https://doi.org/10.1016/j.scitotenv.2024.169881

35 Todd, M. J., Muneepeerakul, R., Pumo, D., Azaele, S., Miralles-Wilhelm, F., Rinaldo, A. & Rodriguez-Iturbe, I. Hydrological drivers of wetland vegetation community distribution within Everglades National Park, Florida. *Advances in Water Resources* **33**, 1279-1289 (2010). https://doi.org/10.1016/j.advwatres.2010.04.003

36 Medina-Gómez, I., Villalobos-Zapata, G. J. & Herrera-Silveira, J. A. Spatial and Temporal Hydrological Variations in the Inner Estuaries of a Large Coastal Lagoon of the Southern Gulf of Mexico. *Journal of Coastal Research* **316**, 1429-1438 (2015). https://doi.org/10.2112/jcoastres-

d-13-00226.1

37 Chowdhury, M. A. W., Varela, S., Roy, S., Rahman, M. M., Noman, M., Haidar, I. K. A. & Müller, J. Favourable climatic niche in low elevations outside the flood zone characterises the distribution pattern of venomous snakes in Bangladesh. *Journal of Tropical Ecology* **38**, 437-450 (2022). https://doi.org/10.1017/s0266467422000359

38 Rogers, K., Zawadzki, A., Mogensen, L. A. & Saintilan, N. Coastal Wetland Surface Elevation Change Is Dynamically Related to Accommodation Space and Influenced by Sedimentation and Sea-Level Rise Over Decadal Timescales. *Frontiers in Marine Science* **9** (2022). https://doi.org/10.3389/fmars.2022.807588

39 Richey, A., Oberbauer, S. F., Castañeda-Moya, E., Troxler, T., Kominoski, J. S., Olivas, P. & Malone, S. L. Sea-level rise and freshwater management are reshaping coastal landscapes. *Journal of Environmental Management* **387** (2025). https://doi.org/10.1016/j.jenvman.2025.125842

40 Paul, S., Das, C. S. & Chaudhuri, S. Seasonal vertical accretion in different hydro-geomorphic environments of Indian Sundarban: Assessing the role of mangroves in mitigating sea level rise impacts. *Geomorphology* **467** (2024). https://doi.org/10.1016/j.geomorph.2024.109493

41 Timm, M. R. & Araújo, R. J. Comparisons of south Florida's seawall and natural mangrove stands reveal similar structural attributes. *Urban Forestry & Urban Greening* **32**, 7-20 (2018). https://doi.org/10.1016/j.ufug.2018.03.013

42 Timmiss, L. A., Martin, J. M., Murray, N. J., Welbergen, J. A., Westcott, D., McKeown, A. & Kingsford, R. T. Threatened but not conserved: flying-fox roosting and foraging habitat in Australia. *Australian Journal of Zoology* **68**, 226-233 (2021). https://doi.org/10.1071/zo20086

43 Kauffman, J. B., Heider, C., Cole, T. G., Dwire, K. A. & Donato, D. C. Ecosystem Carbon Stocks of Micronesian Mangrove Forests. *Wetlands* **31**, 343-352 (2011). https://doi.org/10.1007/s13157-011-0148-9

44 Xu, Y., He, Y., Egidi, E., Franks, A. E., Tang, C. & Xu, J. Pentachlorophenol alters the acetate-assimilating microbial community and redox cycling in anoxic soils. *Soil Biology and Biochemistry* **131**, 133-140 (2019). https://doi.org/10.1016/j.soilbio.2019.01.008

45 Della Patrona, L., Marchand, C., Hubas, C., Molnar, N., Deborde, J. & Meziane, T. Meiofauna distribution in a mangrove forest exposed to shrimp farm effluents (New Caledonia). *Mar Environ Res* **119**, 100-113 (2016). https://doi.org/10.1016/j.marenvres.2016.05.028

46 Cabral, L., Júnior, G. V. L., Pereira de Sousa, S. T., Dias, A. C. F., Lira Cadete, L., Andreote, F. D., Hess, M. & de Oliveira, V. M. Anthropogenic impact on mangrove sediments triggers differential responses in the heavy metals and antibiotic resistomes of microbial communities. *Environmental Pollution* **216**, 460-469 (2016). https://doi.org/10.1016/j.envpol.2016.05.078

47 Méndez, N. Assessing anthropogenic disturbance in Estero de Urías coastal lagoon through the lens of annelid distribution. *Bulletin of Marine Science* **97**, 89-104 (2021). https://doi.org/10.5343/bms.2020.0035

48 Luo, G., Liu, C., Luo, J., Wei, H., Wei, D., Xing, Y. & Sun, X. Heavy metals fate in mangrove wetlands: Integrated insights into sediment-microbe-plant interactions and fraction control. *Journal of Hazardous Materials* **499** (2025). https://doi.org/10.1016/j.jhazmat.2025.140191

49 Kohan, A., Badbardast, Z. & Kohan, A. Effects of shrimp effluents on mudskippers (Gobiidae: Oxudercinae) in the northern Persian Gulf. *Mar Environ Res* **136**, 174-178 (2018). https://doi.org/10.1016/j.marenvres.2018.02.014

50 Zhang, L., Wang, S., Jian, Q., Zhang, P., Lu, Y. & Liu, H. Tidal variation shaped microplastic

enrichment patterns in mangrove blue carbon ecosystem of northern Beibu Gulf, China. *Frontiers in Marine Science* **9** (2022). https://doi.org/10.3389/fmars.2022.927884

51 Kit-Ling Lam , Y.-H. L. <Lam 等 - 2023 - The impact of anthropogenic pollution on Tidal water quality in mangrove wetlands.pdf>. https://doi.org/10.3390/jmse11122374

52 Srichandan, S., Baliarsingh, S. K., Lotliker, A. A., Sahu, B. K., Roy, R. & Nair, T. M. B. Unravelling tidal effect on zooplankton community structure in a tropical estuary. *Environ Monit Assess* **193**, 362 (2021). https://doi.org/10.1007/s10661-021-09112-z

53 Aggrey-Fynn, J. & Siaw Gyimah, D. Tidal influence on Fish Faunal Distribution and Species Diversity in Kakum Estuary, Ghana. *Momona Ethiopian Journal of Science* **16**, 296-314 (2024). https://doi.org/10.4314/mejs.v16i2.8

54 Song, L., Wang, Q., Wang, P. & Wu, J. Benthic bacterial communities and bacteria–environment interactions after Kandelia obovata introduction and Spartina alterniflora invasion in Yueqing Bay, China. *Regional Studies in Marine Science* **58** (2023). https://doi.org/10.1016/j.rsma.2022.102787

55 Molnar, N., Welsh, D. T., Marchand, C., Deborde, J. & Meziane, T. Impacts of shrimp farm effluent on water quality, benthic metabolism and N-dynamics in a mangrove forest (New Caledonia). *Estuarine, Coastal and Shelf Science* **117**, 12-21 (2013). https://doi.org/10.1016/j.ecss.2012.07.012

56 Clemente, C. C. C., Paresque, K. & Santos, P. J. P. Impact of plastic bags on the benthic system of a tropical estuary: An experimental study. *Mar Pollut Bull* **178**, 113623 (2022). https://doi.org/10.1016/j.marpolbul.2022.113623

57 Jayapala, H. P. S., Jayasiri, H. B., Ranatunga, R., Perera, I. & Bellanthudawa, B. K. A. Ecological ramifications of marine debris in mangrove ecosystems: Estimation of substrate coverage and physical effects of marine debris on mangrove ecosystem in Negombo Lagoon, Sri Lanka. *Mar Pollut Bull* **201**, 116184 (2024). https://doi.org/10.1016/j.marpolbul.2024.116184

58 Winterwerp, J. C., Albers, T., Anthony, E. J., Friess, D. A., Mancheño, A. G., Moseley, K., Muhari, A., Naipal, S., Noordermeer, J., Oost, A., Saengsupavanich, C., Tas, S. A. J., Tonneijck, F. H., Wilms, T., Van Bijsterveldt, C., Van Eijk, P., Van Lavieren, E. & Van Wesenbeeck, B. K. Managing erosion of mangrove-mud coasts with permeable dams – lessons learned. *Ecological Engineering* **158** (2020). https://doi.org/10.1016/j.ecoleng.2020.106078

59 Osorio-Cano, J. D., Osorio, A. F. & Peláez-Zapata, D. S. Ecosystem management tools to study natural habitats as wave damping structures and coastal protection mechanisms. *Ecological Engineering* **130**, 282-295 (2019). https://doi.org/10.1016/j.ecoleng.2017.07.015

60 S, A. A., K.R, M., C, R., John, S., G, S., Nair, R. C., K.S, A., K, S. & M.P, P. Modelling of sediment plume associated with the capital dredging for sustainable mangrove ecosystem in the Old Mangalore Port, Karnataka, India. *Regional Studies in Marine Science* **56** (2022). https://doi.org/10.1016/j.rsma.2022.102693

61 Schwarz, C., van Rees, F., Xie, D., Kleinhans, M. G. & van Maanen, B. Salt marshes create more extensive channel networks than mangroves. *Nat Commun* **13**, 2017 (2022). https://doi.org/10.1038/s41467-022-29654-1

62 Tine, M., Diop, P. & Diadhiou, H. D. Benthic Fauna Assessment along the Navigation Channel from the Mouth of the Casamance Estuary to Ziguinchor City. *Conservation* **2**, 367-387 (2022). https://doi.org/10.3390/conservation2020025

63 Chacin, D. H., Giery, S. T., Yeager, L. A., Layman, C. A. & Brian Langerhans, R. Does hydrological

fragmentation affect coastal bird communities? A study from Abaco Island, The Bahamas. *Wetlands Ecology and Management* **23**, 551-557 (2014). https://doi.org/10.1007/s11273-014-9389-8

64 Dash, B., Rout, S. S., Lovaraju, A., Charan Kumar, B., Bharati, A., Ganesh, T., Satyanarayana, B., Raman, A. V., Rakhesh, M. & Raut, D. Macrobenthic community of a tropical bay system revisited: Historical changes in response to anthropogenic forcing. *Mar Pollut Bull* **171**, 112775 (2021). https://doi.org/10.1016/j.marpolbul.2021.112775

65 Friis, G. & Burt, J. A. Evolution of mangrove research in an extreme environment: Historical trends and future opportunities in Arabia. *Ocean & Coastal Management* **195** (2020). https://doi.org/10.1016/j.ocecoaman.2020.105288

66 Wang, H., Galbraith, E. & Convertino, M. Algal Bloom Ties: Spreading Network Inference and Extreme Eco-Environmental Feedback. *Entropy (Basel)* **25** (2023). https://doi.org/10.3390/e25040636

67 Babcock, R. C., Bustamante, R. H., Fulton, E. A., Fulton, D. J., Haywood, M. D. E., Hobday, A. J., Kenyon, R., Matear, R. J., Plagányi, E. E., Richardson, A. J. & Vanderklift, M. A. Severe Continental-Scale Impacts of Climate Change Are Happening Now: Extreme Climate Events Impact Marine Habitat Forming Communities Along 45% of Australia's Coast. *Frontiers in Marine Science* **6** (2019). https://doi.org/10.3389/fmars.2019.00411

68 Osland, M. J., Day, R. H., Michot, T. C. & Lambrinos, J. Frequency of extreme freeze events controls the distribution and structure of black mangroves (Avicennia germinans) near their northern range limit in coastal Louisiana. *Diversity and Distributions* **26**, 1366-1382 (2020). https://doi.org/10.1111/ddi.13119

69 Machava-António, V. C. E., Mabilana, H., Macamo, C., Fernando, A., Santos, R., Bandeira, S. & Paula, J. Massive mangrove dieback due to extreme weather impact - case of Maputo River Estuary, Mozambique. *Regional Studies in Marine Science* **78** (2024). https://doi.org/10.1016/j.rsma.2024.103770

70 Chen, G., Gu, X., Liu, Y., Wang, W. & Wang, M. Responses of a soil mollusk community to an extreme cold event. *Applied Soil Ecology* **167** (2021). https://doi.org/10.1016/j.apsoil.2021.104067

71 Servino, R. N., Gomes, L. E. O. & Bernardino, A. F. Extreme weather impacts on tropical mangrove forests in the Eastern Brazil Marine Ecoregion. *Sci Total Environ* **628-629**, 233-240 (2018). https://doi.org/10.1016/j.scitotenv.2018.02.068

72 Cahoon, D. R., Hensel, P., Rybczyk, J., McKee, K. L., Proffitt, C. E. & Perez, B. C. Mass tree mortality leads to mangrove peat collapse at Bay Islands, Honduras after Hurricane Mitch. *Journal of Ecology* **91**, 1093-1105 (2003). https://doi.org/10.1046/j.1365-2745.2003.00841.x

73 Cahoon, D. R. Measuring and Interpreting the Surface and Shallow Subsurface Process Influences on Coastal Wetland Elevation: A Review. *Estuaries and Coasts* **47**, 1708-1734 (2024). https://doi.org/10.1007/s12237-024-01332-z

74 Scheffel, W. A., Heck, K. L. & Johnson, M. W. Tropicalization of the Northern Gulf of Mexico: Impacts of Salt Marsh Transition to Black Mangrove Dominance on Faunal Communities. *Estuaries and Coasts* **41**, 1193-1205 (2017). https://doi.org/10.1007/s12237-017-0334-y

75 Harada, Y., Fry, B., Lee, S. Y., Maher, D. T., Sippo, J. Z. & Connolly, R. M. Stable isotopes indicate ecosystem restructuring following climate-driven mangrove dieback. *Limnology and Oceanography* **65**, 1251-1263 (2019). https://doi.org/10.1002/lno.11387

76 Mulla, S., Singh, S. K. & Ahmed, R. Assessing the impact of climate change on land-falling tropical cyclones (LFTCs) over the North Indian Ocean (NIO) and their effects on coastal agriculture in Maharashtra: A case study. *Tropical Cyclone Research and Review* **14**, 132-144 (2025). https://doi.org/10.1016/j.tcrr.2025.04.003

77 Nigrelli, L. & Thines, M. Tropical oomycetes in the German Bight – Climate warming or overlooked diversity? *Fungal Ecology* **6**, 152-160 (2013). https://doi.org/10.1016/j.funeco.2012.11.003

78 Armitage, A. R., Weaver, C. A., Whitt, A. A. & Pennings, S. C. Effects of mangrove encroachment on tidal wetland plant, nekton, and bird communities in the Western Gulf of Mexico. *Estuarine, Coastal and Shelf Science* **248** (2021). https://doi.org/10.1016/j.ecss.2020.106767

79 Goeke, J. A. & Armitage, A. R. Coastal woody encroachment reduces food quality for basal consumers. *Ecosphere* **12** (2021). https://doi.org/10.1002/ecs2.3511

80 Armitage, A. R., Highfield, W. E., Brody, S. D. & Louchouarn, P. The contribution of mangrove expansion to salt marsh loss on the Texas Gulf Coast. *PLoS One* **10**, e0125404 (2015). https://doi.org/10.1371/journal.pone.0125404

81 Weaver, C. A. & Armitage, A. R. Nutrient enrichment shifts mangrove height distribution: Implications for coastal woody encroachment. *PLoS One* **13**, e0193617 (2018). https://doi.org/10.1371/journal.pone.0193617

82 Sebastian, P., Jane Stean, S., Rabbani Erawan, A. I., Gotama, R., Swarya, I. N., Sparks, L. D., Prasetijo, R. & Prima Prasetyo, A. Quantifying the influence of environmental factors on elasmobranch distribution and abundance in a high-use marine protected area. *Mar Environ Res* **210**, 107317 (2025). https://doi.org/10.1016/j.marenvres.2025.107317

83 Botella, L., Jung, M. H., Rost, M. & Jung, T. Natural Populations from the Phytophthora palustris Complex Show a High Diversity and Abundance of ssRNA and dsRNA Viruses. *J Fungi (Basel)* **8** (2022). https://doi.org/10.3390/jof8111118

84 Osland, M. J., Feher, L. C., Griffith, K. T., Cavanaugh, K. C., Enwright, N. M., Day, R. H., Stagg, C. L., Krauss, K. W., Howard, R. J., Grace, J. B. & Rogers, K. Climatic controls on the global distribution, abundance, and species richness of mangrove forests. *Ecological Monographs* **87**, 341-359 (2017). https://doi.org/10.1002/ecm.1248

85 Wasserman, R. J., Whitfield, A. K., Deyzel, S. H. P., James, N. C. & Hugo, S. Seagrass (Zostera capensis) bed development as a predictor of size structured abundance for a ubiquitous estuary-dependent marine fish species. *Estuarine, Coastal and Shelf Science* **238** (2020). https://doi.org/10.1016/j.ecss.2020.106694

86 Chen, Q., Yuan, H. & Chen, P. Short-term effects of artificial reef construction on the taxonomic diversity and eco-exergy of the macrobenthic faunal community in the Pearl River Estuary, China. *Ecological Indicators* **98**, 772-782 (2019). https://doi.org/10.1016/j.ecolind.2018.12.001

87 Hyde, K. D., Dong, Y., Phookamsak, R., Jeewon, R., Bhat, D. J., Jones, E. B. G., Liu, N.-G., Abeywickrama, P. D., Mapook, A., Wei, D., Perera, R. H., Manawasinghe, I. S., Pem, D., Bundhun, D., Karunarathna, A., Ekanayaka, A. H., Bao, D.-F., Li, J., Samarakoon, M. C., Chaiwan, N., Lin, C.-G., Phutthacharoen, K., Zhang, S.-N., Senanayake, I. C., Goonasekara, I. D., Thambugala, K. M., Phukhamsakda, C., Tennakoon, D. S., Jiang, H.-B., Yang, J., Zeng, M., Huanraluek, N., Liu, J.-K., Wijesinghe, S. N., Tian, Q., Tibpromma, S., Brahmanage, R. S., Boonmee, S., Huang, S.-K., Thiyagaraja, V., Lu, Y.-Z., Jayawardena, R. S., Dong, W., Yang, E.-F., Singh, S. K., Singh, S. M., Rana, S., Lad, S. S., Anand, G., Devadatha, B., Niranjan, M., Sarma, V. V., Liimatainen, K., Aguirre-

Hudson, B., Niskanen, T., Overall, A., Alvarenga, R. L. M., Gibertoni, T. B., Pfliegler, W. P., Horváth, E., Imre, A., Alves, A. L., da Silva Santos, A. C., Tiago, P. V., Bulgakov, T. S., Wanasinghe, D. N., Bahkali, A. H., Doilom, M., Elgorban, A. M., Maharachchikumbura, S. S. N., Rajeshkumar, K. C., Haelewaters, D., Mortimer, P. E., Zhao, Q., Lumyong, S., Xu, J. & Sheng, J. Fungal diversity notes 1151–1276: taxonomic and phylogenetic contributions on genera and species of fungal taxa. *Fungal Diversity* **100**, 5-277 (2020). https://doi.org/10.1007/s13225-020-00439-5

88 Aumentado, H. D. R., Thilini Chethana, K. W., Jayawardena, R. S., Phukhamsakda, C., Norphanphoun, C., Jones, E. B. G., Bahkali, A. H. & Hyde, K. D. Species diversity of Diaporthe on mangroves: Taxonomic novelties, pathogenic associations, and phylogenetic reassessment of endophytes. *Mycologia* **118**, 47-101 (2026). https://doi.org/10.1080/00275514.2025.2550907

89 Adomat, F., Gischler, E. & Oschmann, W. Taxonomic and taphonomic signatures of mollusk shell concentrations from coastal lagoon environments in Belize, Central America. *Facies* **62** (2015). https://doi.org/10.1007/s10347-015-0454-4

90 Liao, Y., Shou, L., Tang, Y., Gao, A., Chen, Q., Yan, X. & Chen, J. Influence of two non-indigenous plants on intertidal macrobenthic communities in Ximen Island Special Marine Protected Area, China. *Ecological Engineering* **112**, 96-104 (2018). https://doi.org/10.1016/j.ecoleng.2017.12.023

91 Liao, X., Wang, Y., Malghani, S., Zhu, X., Cai, W., Qin, Z. & Wang, F. Methane and nitrous oxide emissions and related microbial communities from mangrove stems on Qi'ao Island, Pearl River Estuary in China. *Sci Total Environ* **915**, 170062 (2024). https://doi.org/10.1016/j.scitotenv.2024.170062

92 Liao, H., Wang, Y., Zhou, Y., Mai, Z., Wang, H., Zhou, W., Liu, D. & Cheng, H. Mangrove afforestation increases microbial necromass but reduces their contribution to soil carbon pool. *Ecological Indicators* **176** (2025). https://doi.org/10.1016/j.ecolind.2025.113695

93 Lugendo, B. R. & Kimirei, I. A. Anthropogenic nitrogen pollution in mangrove ecosystems along Dar es Salaam and Bagamoyo coasts in Tanzania. *Mar Pollut Bull* **168**, 112415 (2021). https://doi.org/10.1016/j.marpolbul.2021.112415

94 Tanu, F. Z., Hinokidani, K., Takahashi, S., Asakura, Y., Hakim, A. & Nakanishi, Y. Anthropogenic nitrogen accumulation potential of Okinawa mangroves in Japan. *Discover Environment* **2** (2024). https://doi.org/10.1007/s44274-024-00145-y

95 Luo, L., Meng, H., Wu, R. N. & Gu, J. D. Impact of nitrogen pollution/deposition on extracellular enzyme activity, microbial abundance and carbon storage in coastal mangrove sediment. *Chemosphere* **177**, 275-283 (2017). https://doi.org/10.1016/j.chemosphere.2017.03.027

96 Chen, J., Zhou, H. C., Wang, C., Zhu, C. Q. & Tam, N. F. Short-term enhancement effect of nitrogen addition on microbial degradation and plant uptake of polybrominated diphenyl ethers (PBDEs) in contaminated mangrove soil. *J Hazard Mater* **300**, 84-92 (2015). https://doi.org/10.1016/j.jhazmat.2015.06.053

97 Bajahmoum, E. A. & Almaghamsi, A. Physicochemical degradation of Avicennia marina mangrove soils in the Red Sea: implications for coastal ecosystem services. *Frontiers in Soil Science* **5** (2025). https://doi.org/10.3389/fsoil.2025.1621591

98 Viswanathan, C., Purvaja, R., Joyson Joe Jeevamani, J., Deepak Samuel, V., Sankar, R., Abhilash, K. R., Gejo Anna, G., Muruganandam, R., Gopi, M., Raja, S., Rocktim Ramen, D., Shesdev, P., Krishnan, P. & Ramesh, R. Salt marsh vegetation in India: Species composition, distribution, zonation pattern and conservation implications. *Estuarine, Coastal and Shelf Science* **242** (2020).

https://doi.org/10.1016/j.ecss.2020.106792

99 Viswanathan, C., Joyson Joe Jeevamani, J., Abhilash, K. R., Amrutha, P. A., Balachandar, K., Manodheepan, K. K., Viswanathan, S., Deepak Samuel, V. & Purvaja, R. A case study on structural development and ecological services of restored mangroves in Adyar Estuary, India. *Nordic Journal of Botany* **2025** (2025). https://doi.org/10.1111/njb.04562

100 Siddiqui, A. S. & Saher, N. U. Heavy metal pollution in sediments and its Biotransference in crabs from mangrove and coastal zones of Pakistan. *Estuarine, Coastal and Shelf Science* **322** (2025). https://doi.org/10.1016/j.ecss.2025.109358

101 Li, R., Li, R., Chai, M., Shen, X., Xu, H. & Qiu, G. Heavy metal contamination and ecological risk in Futian mangrove forest sediment in Shenzhen Bay, South China. *Mar Pollut Bull* **101**, 448-456 (2015). https://doi.org/10.1016/j.marpolbul.2015.09.048

102 Bouchez, A., Pascault, N., Chardon, C., Bouvy, M., Cecchi, P., Lambs, L., Herteman, M., Fromard, F., Got, P. & Leboulanger, C. Mangrove microbial diversity and the impact of trophic contamination. *Mar Pollut Bull* **66**, 39-46 (2013). https://doi.org/10.1016/j.marpolbul.2012.11.015

103 Lee, I. O., Noh, J., Kim, B., Kwon, I., Kim, H., Kwon, B. O., Peng, Y., Hu, Z. & Khim, J. S. Food web dynamics in the mangrove ecosystem of the Pearl River Estuary surrounded by megacities. *Mar Pollut Bull* **189**, 114747 (2023). https://doi.org/10.1016/j.marpolbul.2023.114747

104 Lal, D. M., Sreekanth, G. B., Soman, C., Sharma, A. & Abidi, Z. J. Delineating the food web structure in an Indian estuary during tropical winter employing stable isotope signatures and mixing model. *Environ Sci Pollut Res Int* **30**, 49412-49434 (2023). https://doi.org/10.1007/s11356-023-25549-w

105 Cavanaugh, K. C., Kellner, J. R., Forde, A. J., Gruner, D. S., Parker, J. D., Rodriguez, W. & Feller, I. C. Poleward expansion of mangroves is a threshold response to decreased frequency of extreme cold events. *Proc Natl Acad Sci U S A* **111**, 723-727 (2014). https://doi.org/10.1073/pnas.1315800111

106 Boucek, R. E., Gaiser, E. E., Liu, H. & Rehage, J. S. A review of subtropical community resistance and resilience to extreme cold spells. *Ecosphere* **7** (2016). https://doi.org/10.1002/ecs2.1455

107 Halder, N. K., Merchant, A., Misbahuzzaman, K., Wagner, S. & Mukul, S. A. Why some trees are more vulnerable during catastrophic cyclone events in the Sundarbans mangrove forest of Bangladesh? *Forest Ecology and Management* **490** (2021). https://doi.org/10.1016/j.foreco.2021.119117

108 Taillie, P. J., McCleery, R. A. & Pfeifer, M. Climate relict vulnerable to extinction from multiple climate-driven threats. *Diversity and Distributions* **27**, 2124-2135 (2021). https://doi.org/10.1111/ddi.13380

109 Chen, G., Gu, X., Liu, Y., Shi, X., Wang, W. & Wang, M. Extreme cold events reduce the stability of mangrove soil mollusc community biomass in the context of climate impact. *Environmental Research Letters* **16** (2021). https://doi.org/10.1088/1748-9326/ac1b5b

110 Chen, G., Wang, W., Zhang, Y., Liu, Y., Gu, X., Shi, X. & Wang, M. Abundant and rare species may invoke different assembly processes in response to climate extremes: Implications for biodiversity conservation. *Ecological Indicators* **117** (2020). https://doi.org/10.1016/j.ecolind.2020.106716

111 Kumar, T., Mandal, A., Dutta, D., Nagaraja, R. & Dadhwal, V. K. Discrimination and classification of mangrove forests using EO-1 Hyperion data: a case study of Indian Sundarbans. *Geocarto*

International **34**, 415-442 (2017). https://doi.org/10.1080/10106049.2017.1408699

112 Kumar, A. A., Ali P.H, A. & Bhavan, S. G. Finfish fishery of Ashtamudi Estuary, India- A Ramsar site of International significance. *Regional Studies in Marine Science* **64** (2023). https://doi.org/10.1016/j.rsma.2023.103020

113 Kumar, U., Kaviraj, M., Panneerselvam, P. & Nayak, A. K. Conversion of Mangroves Into Rice Cultivation Alters Functional Soil Microbial Community in Sub-Humid Tropical Paddy Soil. *Frontiers in Environmental Science* **10** (2022). https://doi.org/10.3389/fenvs.2022.858028

114 Veldkornet, D., Rajkaran, A., Paul, S. & Naidoo, G. Oil induces chlorophyll deficient propagules in mangroves. *Mar Pollut Bull* **150**, 110667 (2020). https://doi.org/10.1016/j.marpolbul.2019.110667

115 Yan, Z., Meng, H., Zhang, Q., Bi, Y., Gao, X. & Lei, Y. Effects of cadmium and flooding on the formation of iron plaques, the rhizosphere bacterial community structure, and root exudates in Kandelia obovata seedlings. *Sci Total Environ* **851**, 158190 (2022). https://doi.org/10.1016/j.scitotenv.2022.158190

116 Kang, Y., Kaplan, D. A. & Osland, M. J. Mangrove freeze resistance and resilience across a tropical-temperate transitional zone. *Journal of Ecology* **113**, 94-111 (2024). https://doi.org/10.1111/1365-2745.14440

117 Gauthey, A., Backes, D., Balland, J., Alam, I., Maher, D. T., Cernusak, L. A., Duke, N. C., Medlyn, B. E., Tissue, D. T. & Choat, B. The Role of Hydraulic Failure in a Massive Mangrove Die-Off Event. *Front Plant Sci* **13**, 822136 (2022). https://doi.org/10.3389/fpls.2022.822136

118 Bakshi, M., Ghosh, S., Mahanty, S., Gaine, T. & Chaudhuri, P. Ecotoxicological response of potentially toxic metal (PTM) pollution in estuarine mangrove habitat of Indian Sundarban. *Journal of Earth System Science* **130** (2021). https://doi.org/10.1007/s12040-021-01662-7

119 Rath, S. & Das, S. Oxidative stress-induced DNA damage and DNA repair mechanisms in mangrove bacteria exposed to climatic and heavy metal stressors. *Environ Pollut* **339**, 122722 (2023). https://doi.org/10.1016/j.envpol.2023.122722

120 van Eck, N. J. & Waltman, L. Software survey: VOSviewer, a computer program for bibliometric mapping. *Scientometrics* **84**, 523-538 (2010). https://doi.org/10.1007/s11192-009-0146-3

121 Waltman, L. & van Eck, N. J. A smart local moving algorithm for large-scale modularity-based community detection. *The European Physical Journal B* **86**, 471 (2013). https://doi.org/10.1140/epjb/e2013-40829-0

Supplementary Files

This is a list of supplementary files associated with this preprint. Click to download.

- SupplementaryInformation.docx
- NCOMMS26089419TRSflat.pdf